

## **Response to Editors comments:**

Dear Editor

Thank you very much for your careful reading of our manuscript. We have changed the language edits you suggested and the manuscript has been proofread by a professional language editor. We hope that you are pleased with our revised manuscript.

Regarding the redundancy you mentioned in the method section. As we used bootstrap simulations both in our analysis of coupling between temporal and spatial dynamics in  $F_{opt}$  and  $\alpha$ , and in the parameterisation and evaluation of the GPP model, we have to mention this in both instances. We have, however, removed as much redundant text as we feel is possible.

Yours sincerely,

Torbern Tagesson and co-authors

# Modelling spatial and temporal dynamics of GPP in the Sahel from earth observation based photosynthetic capacity and quantum efficiency

Torbern Tagesson<sup>1</sup>, Jonas Ardo<sup>2</sup>, Bernard Cappelaere<sup>3</sup>, Laurent Kergoat<sup>4</sup>, Abdulkhakim Abdi<sup>2</sup>,  
Stéphanie Horion<sup>1</sup>, Rasmus Fensholt<sup>1</sup>

<sup>1</sup>Department of Geosciences and Natural Resource Management, University of Copenhagen, Øster Voldgade 10, DK-1350 Copenhagen, Denmark; E-Mails: torbern.tagesson@ign.ku.dk, stephanie.horion@ign.ku.dk, rf@ign.ku.dk

<sup>2</sup>Department of Physical Geography and Ecosystem Science, Lund University, Sölvegatan 12, SE- 223 62 Lund, Sweden, E-Mails: jonas.ardo@nateko.lu.se, hakim.abdi@gmail.com

<sup>3</sup>HydroSciences Montpellier, IRD, CNRS, Univ. Montpellier, Montpellier, France, E-Mail: bernard.cappelaere@um2.fr

<sup>4</sup>Geoscience Environnement Toulouse, (CNRS/UPS/IRD), 14 av E Belin, 31400 Toulouse, France, E-Mail: laurent.kergoat@get.obs-mip.fr

*Correspondence to:* Torbern Tagesson (torbern.tagesson@ign.ku.dk)

**Abstract.** It has been shown that vegetation growth in semi-arid regions is important to the global terrestrial CO<sub>2</sub> sink, which indicates the strong need for improved understanding, and spatially explicit estimates of CO<sub>2</sub> uptake (gross primary production (GPP)) in semi-arid ecosystems. This study has three aims: 1) to evaluate the MOD17A2H GPP (collection 6) product against eddy covariance (EC) based GPP for six sites across the Sahel; 2) to characterize relationships between spatial and temporal variability in EC based photosynthetic capacity ( $F_{opt}$ ) and quantum efficiency ( $\alpha$ ) and earth observation (EO) based vegetation indices (normalized difference vegetation index (NDVI); renormalized difference vegetation index (RDVI); enhanced vegetation index (EVI); and shortwave infrared water stress index (SIWSI)); and 3) to study the applicability of EO up-scaled  $F_{opt}$  and  $\alpha$  for GPP modelling purposes. MOD17A2H GPP (collection 6) drastically underestimated GPP ~~strongly~~, most likely because maximum light use efficiency is set too low for semi-arid ecosystems in the MODIS algorithm. Intra-annual dynamics in  $F_{opt}$  ~~was~~ were closely related to SIWSI being sensitive to equivalent water thickness, whereas  $\alpha$  was closely related to RDVI being affected by chlorophyll abundance. Spatial and inter-annual dynamics in  $F_{opt}$  and  $\alpha$  were closely coupled to NDVI and RDVI, respectively. Modelled GPP based on  $F_{opt}$  and  $\alpha$  up-scaled using EO based indices reproduced in situ GPP well for all except a cropped site that was strongly impacted by anthropogenic land use. Up-scaled GPP for the Sahel 2001-2014 was  $736 \pm 39$  g C m<sup>-2</sup> y<sup>-1</sup>. This study indicates the strong applicability of EO as a tool for spatially explicit estimates of GPP,  $F_{opt}$  and  $\alpha$ ; incorporating EO-based  $F_{opt}$  and  $\alpha$  in ~~te~~ dynamic global vegetation models could improve global estimates of vegetation production, ecosystem processes and biogeochemical and hydrological cycles.

38 **Keywords:** Remote sensing, Gross Primary Productivity, MOD17A2H, light use efficiency, photosynthetic capacity,  
39 quantum efficiency

## 40 **1 Introduction**

41 Vegetation growth in semi-arid regions is an important sink for fossil fuel emissions. Mean carbon dioxide (CO<sub>2</sub>)  
42 uptake by terrestrial ecosystems is dominated by highly productive lands, mainly tropical forests, whereas semi-arid  
43 regions are the main biome driving its inter-annual variability (Ahlström et al., 2015; Poulter et al., 2014). Semi-arid  
44 regions even contribute to 60% of the long-term trend in the global terrestrial C sink (Ahlström et al., 2015). It is thus  
45 important to understand long-term variability of vegetation growth in semi-arid areas and ~~their~~ the response of  
46 vegetation to environmental conditions to better quantify and forecast effects of climate change.

47 The Sahel is a semi-arid transition zone between the dry Sahara desert in the North and the humid Sudanian savanna  
48 in the South. The region has experienced numerous severe droughts during ~~over~~ the last decades, which ~~that~~ resulted in  
49 region-wide famines in 1972-1973 and 1984-1985 and localized food shortages across the region in 1990, 2002, 2004,  
50 2011 and 2012 (Abdi et al., 2014; United Nations, 2013). Vegetation production is thereby an important ecosystem  
51 service for livelihoods in the Sahel, but it is under threat. The region is ~~experiencing~~ a strong population growth,  
52 increasing the demand on ecosystem services due to cropland expansion, increased pasture stocking rates and fuelwood  
53 extraction (Abdi et al., 2014).

54 At the same time as we have reports of declining vegetation production, we have contradicting reports of the greening  
55 of the Sahel based on earth observation (EO) data (Dardel et al., 2014; Fensholt et al., 2013). The greening of the Sahel  
56 has mainly been attributed to alleviated drought stress conditions due to increased precipitation since the mid-1990s  
57 (Hickler et al., 2005). Climate is thus another important factor regulating vegetation production. Semi-arid regions, such  
58 as the Sahel, are particularly vulnerable to climate fluctuations due to their dependency on moisture.

59 Estimation of gross primary production (GPP), i.e. uptake of atmospheric CO<sub>2</sub> by vegetation, is still a major challenge  
60 ~~within~~ for the remote sensing of ecosystem services. Gross primary production is a main driver of ecosystem services  
61 such as climate regulation, carbon (C) sequestration, C storage, food production, ~~or~~ and livestock grassland production.  
62 Within EO, spatial quantification of GPP generally involves light use efficiency (LUE), defined as the conversion  
63 efficiency of absorbed solar light into CO<sub>2</sub> uptake (Monteith, 1972, 1977). It has been shown that LUE varies in space  
64 and time due to factors such as plant functional type, drought and temperature, nutrient levels and physiological  
65 limitations of photosynthesis (Garbulska et al., 2010; Paruelo et al., 2004; Kergoat et al., 2008). The LUE concept has  
66 been applied using ~~through~~ various methods, either by using a biome-specific LUE constant (Ruimy et al., 1994), or by  
67 modifying a maximum LUE using meteorological variables (Running et al., 2004).

68 An example of ~~a~~ LUE based model is the standard GPP product from the Moderate Resolution Imaging  
69 Spectroradiometer (MODIS) sensor (MOD17A2). Within the model, absorbed photosynthetically active radiation  
70 (PAR) is estimated as a product of the fraction of PAR absorbed by green vegetation (FPAR from MOD15A2)  
71 multiplied with daily PAR from the meteorological data of the Global Modeling and Assimilation Office (GMAO). A  
72 set of maximum LUE parameters specified for each biome are extracted from a Biome Properties Look-Up Table  
73 (BPLUT). Then maximum LUE is modified depending on air temperature (T<sub>air</sub>) and vapour pressure deficit (VPD)  
74 (Running et al., 2004). Sjöström et al. (2013) evaluated the MOD17A2 product (collection 5.1) for Africa, and showed

75 that it underestimated GPP for semi-arid savannas in the Sahel. Explanations for this underestimation were that the  
76 assigned maximum LUE from BPLUT was set too low and that there were uncertainties in the FPAR product  
77 (MOD15A2). Recently, a new collection of MOD17A2 at a 500 m spatial resolution was released (MOD17A2H;  
78 collection 6) with an updated BPLUT, updated GMAO meteorological data, improved quality control and gap-filling  
79 of the FPAR data from MOD15A2 (Running and Zhao, 2015).

80 It has been shown that the LUE method does not perform well in arid conditions and at agricultural sites (Turner et  
81 al., 2005). Additionally, the linearity assumed by the LUE model is not usually ~~not~~ found as the response of GPP to  
82 incoming light follows more of an asymptotic curve (Cannell and Thornley, 1998). Investigating other methods for  
83 remotely determining GPP is thus of great importance, especially for semi-arid environments. Therefore, instead of  
84 LUE, we focus on the light response function of GPP at the canopy scale, and spatial and temporal variation of its two  
85 main parameters: maximum GPP under light saturation (canopy-scale photosynthetic capacity;  $F_{opt}$ ); and the initial  
86 slope of the light response function (canopy-scale quantum efficiency;  $\alpha$ ) (Falge et al., 2001; Tagesson et al., 2015a).  
87 Photosynthetic capacity is a measure of the maximum rate at which the canopy can fix  $CO_2$  during photosynthesis  
88 ( $\mu mol CO_2 m^{-2} s^{-1}$ ), whereas  $\alpha$  is the amount of  $CO_2$  fixed per incoming PAR ( $\mu mol CO_2 \mu mol PAR^{-1}$ ). ~~Just to~~ clarify  
89 the difference in LUE and  $\alpha$  in this study, LUE ( $\mu mol CO_2 \mu mol PAR^{-1}$ ) is the slope of a linear fit between  $CO_2$   
90 uptake and absorbed PAR, whereas  $\alpha$  ( $\mu mol CO_2 \mu mol PAR^{-1}$ ) is the initial slope of an asymptotic curve against  
91 incoming PAR.

92 It has been proven that  $F_{opt}$  and  $\alpha$  are closely related to chlorophyll abundance due to their coupling with the electron  
93 transport rate (Ide et al., 2010). Additionally, in semi-arid ecosystems, water availability is generally considered to be  
94 the main limiting factor affecting intra-annual dynamics of vegetation growth (Fensholt et al., 2013; Hickler et al.,  
95 2005; Tagesson et al., 2015b). Several remote sensing studies have established relationships between remotely sensed  
96 vegetation indices and ecosystem properties such as chlorophyll abundance and equivalent water thickness (Yoder and  
97 Pettigrew-Crosby, 1995; Fensholt and Sandholt, 2003). In this study, we will analyse if whether EO vegetation indices  
98 can be used ~~for~~ to up-scaling  $F_{opt}$  and  $\alpha$  and investigate if whether this could offer a promising way to map GPP in semi-  
99 arid areas. This potential will be analysed by the use of detailed ground observations from six eddy covariance (EC)  
100 flux tower sites across the Sahel.

101 The three aims of this study are:

- 102 1) To investigate if whether the recently released MOD17A2H GPP (collection 6) product is better at capturing  
103 GPP for the Sahel than collection 5.1. We hypothesize that the MOD17A2H GPP (collection 6) product will  
104 estimate GPP well for the six Sahelian EC sites, because of major changes ~~done~~ made in comparison to  
105 collection 5.1 (Running and Zhao, 2015).
- 106 2) To characterize the relationships between spatial and temporal variability in  $F_{opt}$  and  $\alpha$  and remotely sensed  
107 vegetation indices. We hypothesize that EO vegetation indices that are closely related to chlorophyll  
108 abundance will be most strongly coupled with spatial and inter-annual dynamics in  $F_{opt}$  and  $\alpha$ , whereas  
109 vegetation indices closely related to equivalent water thickness will be most strongly coupled with intra-annual  
110 dynamics in  $F_{opt}$  and  $\alpha$  across the Sahel.
- 111 3) To evaluate the applicability of a GPP model based on the light response function using EO vegetation indices  
112 and incoming PAR as input data.

113

114 **2 Materials and Methods**

115 **2.1 Site description**

116 | The Sahel stretches from the Atlantic Ocean in the west to the Red Sea in the east. The northern border towards [the](#)  
117 | Sahara and the southern border towards the humid Sudanian Savanna are defined by the 150 and 700 mm isohyets,  
118 | respectively (Fig. 1) (Prince et al., 1995). Tree and shrub canopy cover is now generally low (< 5%) and dominated by  
119 | species of *Balanites*, *Acacia*, *Boscia* and *Combretaceae* (Rietkerk et al., 1996). Annual grasses such as *Schoenefeldia*  
120 | *gracilis*, *Dactyloctenium aegypticum*, *Aristida mutabilis*, and *Cenchrus biflorus* dominate the herbaceous layer, but  
121 | perennial grasses such as *Andropogon gayanus*, *Cymbopogon schoenanthus* can also be found (Rietkerk et al., 1996; de  
122 | Ridder et al., 1982). From the FLUXNET database (Baldocchi et al., 2001) we selected the six available measurement  
123 | sites with EC based CO<sub>2</sub> flux data from [the](#) Sahel (Table 1; Fig. 1). The sites represent a variety of ecosystems present  
124 | in the region, from dry fallow bush savanna to seasonally inundated acacia forest. For a full description of the  
125 | measurement sites, we refer to Tagesson et al. (2016a) and references in Table 1.

126 <Table 1>

127 <Figure 1>

128

129 **2.2 Data collection**

130 **2.2.1 Eddy covariance and hydrometeorological in situ data**

131 Eddy covariance and hydrometeorological data originating from the years between 2005 and 2013 were collected from  
132 | the principal investigators of the measurement sites (Tagesson et al., 2016a). The EC sensor set-up consisted of open-  
133 | path CO<sub>2</sub>/H<sub>2</sub>O infrared gas analysers and 3-axis sonic anemometers. Data were collected at 20 Hz rate and statistics  
134 | were calculated for 30-minute periods. For a full description of [the](#) sensor set-up and post processing of EC data, see [the](#)  
135 | references in Table 1. Final fluxes were filtered according to quality flags provided by FLUXNET and outliers were  
136 | filtered according to Papale et al. (2006). We extracted the original net ecosystem exchange (NEE) data without any  
137 | gap-filling or partitioning of NEE to GPP and ecosystem respiration. The collected hydrometeorological data were: air  
138 | temperature ( $T_{\text{air}}$ ; °C), rainfall (P; mm), relative air humidity (Rh; %), soil moisture at 0.1 m depth (SWC; % volumetric  
139 | water content), incoming global radiation ( $R_g$ ; W m<sup>-2</sup>), incoming photosynthetically active radiation (PAR;  $\mu\text{mol m}^{-2} \text{s}^{-1}$ ),  
140 | VPD (hPa), peak dry weight biomass (g dry weight m<sup>-2</sup>), C3/C4 species ratio, and soil conditions (nitrogen and C  
141 | concentration; %). For a full description of [the](#) collected data and sensor set-up, see Tagesson et al. (2016a).

142

143 **2.2.2 Earth Observation data and gridded ancillary data**

144 | Composite products from MODIS/Terra covering [the](#) Sahel were acquired at Reverb ECHO (NASA, 2016). Collected  
145 | products were GPP (MOD17A2H; collection 6), nadir bidirectional reflectance distribution function adjusted  
146 | reflectance (NBAR) (8-day composites; MCD43A4; collection 5.1) at 500×500 m<sup>2</sup> spatial resolution, the normalized  
147 | difference vegetation index (NDVI) and the enhanced vegetation index (EVI) (16-day composites; MOD13Q1;  
148 | collection 6) at 250×250 m<sup>2</sup> spatial resolution. The NBAR product was preferred over the reflectance product  
149 | (MOD09A1) in order to avoid variability caused by varying sun and sensor viewing geometry (Huber et al., 2014;  
150 | Tagesson et al., 2015c). We extracted the median of 3x3 pixels centred at the location of each EC tower. Time series of  
151 | EO products were filtered according to MODIS quality control data; MOD17A2H is a gap-filled and filtered product,

152 QC data from MCD43A2 were used for filtering of MCD43A4; and bit 2-5 (highest –decreasing quality) was used for  
153 MOD13Q1. Finally, data were gap-filled to daily values using linear interpolation.

154 We downloaded ERA Interim reanalysis PAR at the ground surface ( $W m^{-2}$ ) with a spatial resolution of  $0.25^{\circ} \times 0.25^{\circ}$   
155 accumulated for each 3-hour period from 2000-2015 from the European Centre for Medium-Range Weather Forecasts  
156 (ECMWF) (Dee et al., 2011; ECMWF, 2016a).

157

## 158 2.3 Data handling

### 159 2.3.1 Intra-annual dynamics in photosynthetic capacity and quantum efficiency

160 To estimate daily values of EC based  $F_{opt}$  and  $\alpha$ , the asymptotic Mitscherlich light-response function was fitted  
161 between daytime NEE and incoming PAR using a 7-day moving window with a 1-day time step:

$$162 \quad NEE = -(F_{opt}) \times \left(1 - e^{\left(\frac{-\alpha \times PAR}{F_{opt}}\right)}\right) + R_d \quad (1)$$

163 where  $F_{opt}$  is  $CO_2$  uptake at light saturation (photosynthetic capacity;  $\mu mol CO_2 m^{-2} s^{-1}$ ),  $R_d$  is dark respiration  
164 ( $\mu mol CO_2 m^{-2} s^{-1}$ ); and  $\alpha$  is the initial slope of the light response curve (quantum efficiency;  $\mu mol CO_2 \mu mol PAR^{-1}$ )  
165 (Falge et al., 2001). By subtracting  $R_d$  from Eq. 1, the function was forced through zero and GPP was thereby  
166 estimated. To ensure a high quality of fitted parameters, parameters were excluded from the analysis when fitting  
167 was insignificant (p-value > 0.05); and when they were out of range ( $F_{opt}$  and  $\alpha$  > peak value of the rainy season times  
168 1.2). Additionally, outliers were filtered following the method by Papale et al. (2006) using a 30-day moving window  
169 with a 1-day time step.

170

### 171 2.3.2 Vegetation indices

172 The maximum absorption in red wavelengths generally occurs at 682 nm as this is the peak absorption for chlorophyll a  
173 and b (Thenkabail et al., 2000), which makes vegetation indices that include the red band sensitive to chlorophyll  
174 abundance. By far the most common vegetation index is NDVI (Rouse et al., 1974):

$$175 \quad NDVI = \frac{(\rho_{NIR} - \rho_{red})}{(\rho_{NIR} + \rho_{red})} \quad (2)$$

176 where  $\rho_{NIR}$  is the reflectance factor in the near infrared (NIR) band (band 2) and  $\rho_{red}$  is the reflectance factor in the red  
177 band (band 1). Near infrared radiance is reflected by leaf cells since absorption of these wavelengths would result in  
178 overheating of the plant, whereas red radiance is absorbed by chlorophyll and its accessory pigments (Gates et al.,  
179 1965). Normalization is done to reduce effects of atmospheric errors, solar zenith angles; and sensor viewing geometry,  
180 as well as to increase the vegetation signal (Qi et al., 1994; Inoue et al., 2008).

181 A well-known deficiency of NDVI is problems of index saturation at high biomass because absorption of red light at  
182 ~670 nm peaks at higher biomass loads, whereas NIR reflectance continues to increase due to multiple scattering effects  
183 (Mutanga and Skidmore, 2004; Jin and Eklundh, 2014). By reducing atmospheric and soil background influences, EVI  
184 is designed to increase the signal from the vegetation and maintain sensitivity in high biomass regions (Huete et al.,  
185 2002).

$$186 \quad EVI = G \frac{(\rho_{NIR} - \rho_{red})}{(\rho_{NIR} + C_1 \rho_{red} - C_2 \rho_{blue} + L)} \quad (3)$$

187 where  $\rho_{blue}$  is the reflectance factor in the blue band (band 3). The coefficients  $C_1=6$  and  $C_2=7.5$  correct for atmospheric  
188 influences, while  $L=1$  adjusts for the canopy background. The factor  $G=2.5$  is a gain factor.

189 Another attempt to overcome problems of NDVI saturation was proposed by Roujean and Breon (1995), who  
190 suggested the renormalized difference vegetation index (RDVI), ~~that~~which combines advantages of DVI (NIR-red) and  
191 NDVI for low and high vegetation cover, respectively:

$$192 \quad RDVI = \frac{(\rho_{NIR} - \rho_{red})}{\sqrt{(\rho_{NIR} + \rho_{red})}} \quad (4)$$

193 As a non-linear index, RDVI is not only less sensitive to variations in geometrical and optical properties of unknown  
194 foliage but also less affected by solar and viewing geometry (Broge and Leblanc, 2001). The vegetation index RDVI  
195 was calculated based on NBAR bands 1 and 2.

196 The NIR and SWIR bands are affected by the same ground properties, except that SWIR bands are also strongly  
197 sensitive to equivalent water thickness. Fensholt and Sandholt (2003) proposed a vegetation index, the shortwave  
198 infrared water stress index (SIWSI), using NIR and SWIR bands to estimate drought stress for vegetation in semi-arid  
199 environments:

$$200 \quad SIWSI_{12} = \frac{(\rho_{NIR} - \rho_{SWIR12})}{(\rho_{NIR} + \rho_{SWIR12})} \quad (5)$$

$$201 \quad SIWSI_{16} = \frac{(\rho_{NIR} - \rho_{SWIR16})}{(\rho_{NIR} + \rho_{SWIR16})} \quad (6)$$

202 where  $\rho_{swir12}$  is NBAR band 5 (1230-1250 nm) and  $\rho_{swir16}$  is NBAR band 6 (1628-1652 nm). As the vegetation water  
203 content increases, reflectance in SWIR decreases, indicating that low and high SIWSI values point to sufficient water  
204 conditions and drought stress, respectively.

205

### 206 2.3.3 Incoming PAR across the Sahel

207 A modified version of the ERA Interim reanalysis PAR was used in the current study as there was an error in the code  
208 producing these PAR estimates; the estimates were generally too low (ECMWF, 2016b). Accordingly, incoming PAR  
209 at the ground surface from ERA Interim was systematically underestimated even though it followed the pattern of PAR  
210 measured at the six Sahelian EC sites (Fig. S1 in supplementary material). In order to correct for this error, we fitted  
211 and applied an ordinary least squares linear regression between in situ PAR and ERA Interim PAR (Fig. S1). The PAR  
212 produced from this relationship is at the same level as in situ PAR and should be at a correct level even though the  
213 original ERA Interim PAR is actually produced from the red and near infrared part of the spectrum.

214

## 215 2.4 Data analysis

### 216 2.4.1 Coupling temporal and spatial dynamics in photosynthetic capacity and quantum efficiency with 217 explanatory variables

218 The coupling between intra-annual dynamics in  $F_{opt}$  and  $\alpha$  and the vegetation indices for the different measurement sites  
219 were studied using Pearson correlation analysis. As part of the correlation analysis, we used a bootstrap simulation  
220 methodology with 200 iterations from which the mean and the standard deviation of the correlation coefficients were  
221 calculated (Richter et al., 2012). Relationships between intra-annual dynamics in  $F_{opt}$  and  $\alpha$  and the vegetation indices

222 for all sites combined were also analysed. In the analysis for all sites, data were normalized in order to avoid influence  
 223 of spatial and inter-annual variability. Time series of ratios of  $F_{opt}$  and  $\alpha$  ( $F_{opt\_frac}$  and  $\alpha_{frac}$ ) against the annual peak  
 224 values ( $F_{opt\_peak}$  and  $\alpha_{peak}$ ; see below for calculation of annual peak values) were estimated for all sites:

$$225 \quad F_{opt\_frac} = \frac{F_{opt}}{F_{opt\_peak}} \quad (7)$$

$$226 \quad \alpha_{frac} = \frac{\alpha}{\alpha_{peak}} \quad (8)$$

227 The same standardization procedure was used for all vegetation indices ( $VI_{frac}$ ):

$$228 \quad VI_{frac} = \frac{VI}{VI_{peak}} \quad (9)$$

229 where  $VI_{peak}$  is the annual peak values of the vegetation indices (14-day running mean with highest annual value). The  
 230  $\alpha_{frac}$  and  $F_{opt\_frac}$  were correlated with the different  $VI_{frac}$  to investigate the coupling between intra-annual dynamics in  
 231  $F_{opt}$  and  $\alpha$  and the vegetation indices for all sites.

232 Regression trees were used to fill gaps in the daily estimates of  $F_{opt}$  and  $\alpha$ . One hundred tree sizes were chosen based  
 233 on 100 cross-validation runs, and these trees were then used to estimate  $F_{opt}$  and  $\alpha$  following the method in  
 234 De'ath and Fabricius (2000). We used SWC, VPD,  $T_{air}$ , PAR, and the vegetation index with the strongest correlation  
 235 with intra-annual dynamics as explanatory variables in the analysis. In the analysis for all sites, the same  
 236 standardization procedure as done for  $F_{opt}$ ,  $\alpha$ , and the vegetation indices was done for the hydrometeorological  
 237 variables. The 100  $F_{opt}$  and  $\alpha$  output subsets from the regression trees were averaged and used for filling gaps in the  
 238 time series of  $F_{opt}$  and  $\alpha$ . From these time series, we estimated annual peak values of  $F_{opt}$  and  $\alpha$  ( $F_{opt\_peak}$  and  $\alpha_{peak}$ ) as  
 239 the 14-day running mean with the highest annual value. To investigate spatial and inter-annual variability in  $F_{opt}$  and  $\alpha$   
 240 across the measurement sites of the Sahel,  $F_{opt\_peak}$  and  $\alpha_{peak}$  were correlated with the annual sum of  $P_{\geq}$  yearly means of  
 241  $T_{air}$ , SWC, RH, VPD, and  $R_g$ ; annual peak values of biomass, soil nitrogen and C concentrations; the C3/C4 ratio;  
 242 and  $VI_{peak}$ .

243

#### 244 2.4.2 Parameterization and evaluation of the GPP model and evaluation of the MODIS GPP

245 Based on the basis of Eq. 1 and the outcome of the statistical analysis previously described under subsection 2.4.1 (for  
 246 results, see subject. 3.2), a model for estimating GPP across the Sahel was created:

$$247 \quad GPP = -F_{opt} \times \left(1 - e^{\left(\frac{-\alpha \times PAR}{F_{opt}}\right)}\right) \quad (10)$$

248 Firstly,  $F_{opt\_peak}$  and  $\alpha_{peak}$  were estimated spatially and inter-annually using linear regression functions fitted against the  
 249 vegetation indices with strongest relationships to spatial and inter-annual variability in  $F_{opt\_peak}$  and  $\alpha_{peak}$  for all sites.  
 250 Secondly, exponential regression functions were established for  $F_{opt\_frac}$  and  $\alpha_{frac}$  with the vegetation index with the  
 251 strongest relationships to intra-annual variability of  $F_{opt\_frac}$  and  $\alpha_{frac}$  for all sites. By combining these relationships,  $F_{opt}$   
 252 and  $\alpha$  can be calculated for any day of year and for any point in space across the Sahel:

$$253 \quad F_{opt} = F_{opt\_peak} \times F_{opt\_frac} = \left(k_{Fopt} \times NDVI_{peak} + m_{Fopt}\right) \left(n_{Fopt} \times e^{\left(l_{Fopt} \times RDVI_{frac}\right)}\right) \quad (11)$$



254  $\alpha = \alpha_{\text{peak}} \times \alpha_{\text{frac}} = \left( k_{\alpha} \times \text{RDVI}_{\text{peak}} + m_{\alpha} \right) \left( n_{\alpha} \times e^{(l_{\alpha} \times \text{RDVI}_{\text{frac}})} \right)$  (12)

255 where  $k_{\text{Fopt}}$  and  $k_{\alpha}$  are slopes and  $m_{\text{Fopt}}$  and  $m_{\alpha}$  are intercepts of the linear regressions giving  $F_{\text{opt\_peak}}$  and  $\alpha_{\text{peak}}$ ,  
 256 respectively;  $l_{\text{Fopt}}$  and  $l_{\alpha}$  are coefficients and  $n_{\text{Fopt}}$  and  $n_{\alpha}$  are intercepts of the exponential regressions giving  $F_{\text{opt\_frac}}$  and  
 257  $\alpha_{\text{frac}}$ , respectively. Equations 11 and 12 were inserted into Eq. 10, and GPP ~~were~~ thereby estimated as:

258 
$$\text{GPP} = - \left( F_{\text{opt\_peak}} \times F_{\text{opt\_frac}} \right) \times \left( 1 - e^{- \left( \frac{(-\alpha_{\text{peak}} \times \alpha_{\text{frac}}) \times \text{PAR}}{F_{\text{opt\_peak}} \times F_{\text{opt\_frac}}} \right)} \right) = - \left( \left( k_{\text{Fopt}} \times \text{NDVI}_{\text{peak}} + m_{\text{Fopt}} \right) \left( n_{\text{Fopt}} \times e^{(l_{\text{Fopt}} \times \text{RDVI}_{\text{frac}})} \right) \right)$$
  

$$\times \left( 1 - e^{- \left( \frac{(-k_{\alpha} \times \text{RDVI}_{\text{peak}} + m_{\alpha}) \left( n_{\alpha} \times e^{(l_{\alpha} \times \text{RDVI}_{\text{frac}})} \right) \times \text{PAR}}{\left( k_{\text{Fopt}} \times \text{NDVI}_{\text{peak}} + m_{\text{Fopt}} \right) \left( l_{\text{Fopt}} \times \text{RDVI}_{\text{frac}} + n_{\text{Fopt}} \right)} \right)} \right)$$
 (13)

259 The bootstrap simulation methodology was used when fitting the least-square regression functions for  
 260 parameterization of the GPP model (Richter et al., 2012). For each of the iterations, some of the EC sites were included  
 261 and some were ~~left out~~. The bootstrap simulations generated 200 sets of  $k_{\text{Fopt}}$ ,  $k_{\alpha}$ ,  $m_{\text{Fopt}}$ ,  $m_{\alpha}$ ,  $l_{\text{Fopt}}$ ,  $l_{\alpha}$ ,  $n_{\text{Fopt}}$ ,  $n_{\alpha}$ ,  
 262 and coefficient of determination ( $R^2$ ). Possible errors (e.g. random sampling errors, aerosols, electrical sensor noise,  
 263 filtering and gap-filling errors, clouds, and satellite sensor degradation) can be present in both the predictor and the  
 264 response variables. Hence, we selected reduced major axis regressions to account for errors in both predictor and  
 265 response variables when fitting the regression functions. The regression models were validated against the ~~left-~~  
 266 ~~out~~ sites within the bootstrap simulation methodology by calculating the root-mean-square-error (RMSE), and  
 267 by fitting an ordinary least squares linear regression between modelled and independent variables.

268 Similarly, the MODIS GPP product (MOD17A2H; collection 6) was evaluated against independent GPP from the EC  
 269 sites by calculating the RMSE, and by fitting an ordinary least squares linear regression.

270

### 271 3 Results

#### 272 3.1 Evaluation of the MODIS GPP product

273 There was a strong linear relationship between the MODIS GPP product (MOD17A2H; collection 6) and independent  
 274 GPP (slope=0.17; intercept=0.11 g C m<sup>-2</sup> d<sup>-1</sup>; R<sup>2</sup>=0.69; n=598). However, MOD17A2H strongly underestimated  
 275 independent GPP (Fig. 2), resulting in a high RMSE (2.69 g C m<sup>-2</sup> d<sup>-1</sup>). It can be seen that some points for the Kelma  
 276 site were quite low for MOD17A2H, whereas they were relatively high for the independent GPP (Fig. 2). Kelma is an  
 277 inundated Acacia forest located in a clay soil depression. These differentiated values were found in the beginning of the  
 278 dry season, when the depression was still inundated, whereas the larger area was turning dry.

279 <Figure 2>

280

#### 281 3.2 Intra-annual dynamics in photosynthetic capacity and quantum efficiency

282 Intra-annual dynamics in  $F_{\text{opt}}$  and  $\alpha$  differed in amplitude, but were otherwise similar across the measurement sites in  
 283 the Sahel (Fig. 3). There was no green ground vegetation during the dry season, and the low photosynthetic activity was  
 284 due to few evergreen trees. This resulted in low values for both  $F_{\text{opt}}$  and  $\alpha$  during the dry season. The vegetation  
 285 responded strongly to rainfall, and both  $F_{\text{opt}}$  and  $\alpha$  increased during the early phase of the rainy season. Generally,  $F_{\text{opt}}$   
 286 peaked slightly earlier than  $\alpha$  (average  $\pm$  1 standard deviation: 7  $\pm$  10 days) (Fig. 3).

287 <Figure 3>

288 All vegetation indices described intra-annual dynamics in  $F_{opt}$  reasonably well at all sites (Table 2). The vegetation  
289 index SIWSI<sub>12</sub> had the highest correlation for all sites except Wankama Millet, where it was RDVI. When all sites were  
290 combined, all indices described well seasonality in  $F_{opt}$ , but RDVI had the strongest correlation (Table 2).

291 Intra-annual dynamics in  $\alpha$  were also closely coupled to intra-annual dynamics in the vegetation indices for all sites  
292 (Table 2). For  $\alpha$ , RDVI was the strongest index describing intra-annual dynamics, except for Wankama Fallow, where it  
293 was EVI. When all sites were combined, all indices described well intra-annual dynamics in  $\alpha$ , but RDVI was still the  
294 index with strongest relationship (Table 2).

295 <Table 2>

296 The regression trees used for gap-filling explained the intra-annual dynamics in  $F_{opt}$  and  $\alpha$  well for all sites (Table 3;  
297 Fig. S2 in Supplementary material). The regression trees explained intra-annual dynamics in  $F_{opt}$  better than in  $\alpha$ , and  
298 multi-year sites were better predicted than single year sites (Fig. S2). The main explanatory variables coupled to intra-  
299 annual dynamics in  $F_{opt}$  for all sites across the Sahel were in the order of RDVI, SWC, VPD,  $T_{air}$ , and PAR; and for  $\alpha$   
300 they were RDVI, SWC, VPD and  $T_{air}$  (Table 3). The strong relationship to SWC and VPD indicates drought stress  
301 during periods of low rainfall. For all sites across the Sahel, incorporating hydrometeorological variables increased the  
302 ability to determine intra-annual dynamics in  $F_{opt}$  and  $\alpha$  compared to the ordinary least squares linear regressions against  
303 vegetation indices (Table 2, data given as  $r$ ; Table 3; Fig. 3 and Fig. S2). For all sites, incorporation of these variables  
304 increased  $R^2$  from 0.81 to 0.87 and from 0.74 to 0.84, for  $F_{opt}$  and  $\alpha$ , respectively.

305 <Table 3>

306

### 307 3.3 Spatial and inter-annual dynamics in photosynthetic capacity and quantum efficiency

308 Large spatial and inter-annual variability in  $F_{opt\_peak}$  and  $\alpha_{peak}$  were found across the six measurement sites in the Sahel;  
309  $F_{opt\_peak}$  ranged between 10.1  $\mu\text{mol CO}_2 \text{ m}^{-2} \text{ s}^{-1}$  (Wankama Millet 2005) and 50.0  $\mu\text{mol CO}_2 \text{ m}^{-2} \text{ s}^{-1}$  (Dahra 2010), and  
310  $\alpha_{peak}$  ranged between 0.020  $\mu\text{mol CO}_2 \mu\text{mol PAR}^{-1}$  (Demokeya 2007) and 0.064  $\mu\text{mol CO}_2 \mu\text{mol PAR}^{-1}$  (Dahra 2010)  
311 (Table 4). The average two-week running mean peak values of  $F_{opt}$  and  $\alpha$  for all sites were 26.4  $\mu\text{mol CO}_2 \text{ m}^{-2} \text{ s}^{-1}$  and  
312 0.040  $\mu\text{mol CO}_2 \mu\text{mol PAR}^{-1}$ , respectively. All vegetation indices determined spatial and inter-annual dynamics well in  
313 both  $F_{opt\_peak}$  and  $\alpha_{peak}$  (Table 5);  $F_{opt\_peak}$  was most closely coupled with  $\text{NDVI}_{peak}$ , whereas  $\alpha_{peak}$  was coupled more  
314 closely with  $\text{RDVI}_{peak}$  (Fig. 4).  $F_{opt\_peak}$  also correlated well with peak dry weight biomass, C content in the soil, and  
315 RH, whereas  $\alpha_{peak}$  also correlated well with peak dry weight biomass, and C content in the soil (Table 5).

316 <Table 4>

317 <Table 5>

318 <Figure 4>

319

### 320 3.4 Spatially extrapolated photosynthetic capacity, quantum efficiency, and gross primary production across the 321 Sahel and evaluation of the GPP model

322 The spatially extrapolated  $F_{opt}$ ,  $\alpha$  and GPP averaged over the Sahel for 2001-2014 were  $22.5 \pm 1.7 \mu\text{mol CO}_2 \text{ m}^{-2} \text{ s}^{-1}$ ,  
323  $0.030 \pm 0.002 \mu\text{mol CO}_2 \mu\text{mol PAR}^{-1}$ , and  $736 \pm 39 \text{ g C m}^{-2} \text{ y}^{-1}$ , respectively. At a regional scale, it can be seen that  $F_{opt}$ ,  
324  $\alpha$ , and GPP decreased substantially with latitude (Fig. 5). The highest values were found in south-eastern Senegal,  
325 western Mali, in parts of southern Sudan and on the border between Sudan and South Sudan. Lowest values were found

326 | along the northernmost parts of the Sahel on the border to the Sahara in Mauritania, in northern Mali; and in northern  
327 | Niger.

328 | Modelled GPP was similar to independent GPP on average, and there was a strong linear relationship between  
329 | modelled GPP and independent GPP for all sites (Fig. 6; Table 6). However, when separating the evaluation between  
330 | measurement sites, it can be seen that the model reproduced some sites better than others (Fig. 7; Table 6). Wankama  
331 | Millet was generally overestimated, whereas the model worked well on average for Demokeya but underestimated high  
332 | values (Fig. 7; Table 6). Variability of independent GPP at the other sites was well reproduced by the model (Fig. 7;  
333 | Table 6). The final parameters of the GPP model (Eq. 13) are givenshown in Table 7.

334 | <Figure 5>

335 | <Figure 6>

336 | <Figure 7>

337 | < Table 6>

338 | < Table 7>

339

#### 340 | **4 Discussions**

341 | Our hypothesis that vegetation indices closely related to equivalent water thickness (SIWSI) would be most strongly  
342 | coupled with intra-annual dynamics in  $F_{opt}$  and  $\alpha$  was not rejected for  $F_{opt}$ , since this was the case for all sites except for  
343 | Wankama Millet (Table 2). However, our hypothesis was rejected for  $\alpha$ , since it was more closely related to vegetation  
344 | indices related to of chlorophyll abundance (RDVI and EVI). In the Sahel, soil moisture conditions in the early rainy  
345 | season are important for vegetation growth and during this phase vegetation is especially vulnerable to drought  
346 | conditions (Rockström and de Rouw, 1997; Tagesson et al., 2016a; Mbow et al., 2013). Photosynthetic capacity ( $F_{opt}$ )  
347 | peaked earlier in the rainy season than  $\alpha$  did (Fig. 3), thereby explaining the close relationship of  $F_{opt}$  to SIWSI. Leaf  
348 | area index increased over the growing season and leaf area index is closely coupled with vegetation indices related to  
349 | chlorophyll abundance (Tagesson et al., 2009). The increase in leaf area index increased canopy level quantum  
350 | efficiency ( $\alpha$ ), which thereby explainsing the closer relationship of  $\alpha$  to RDVI.

351 | Our hypothesis that vegetation indices closely related to chlorophyll abundance would be most strongly coupled with  
352 | spatial and inter-annual dynamics in  $F_{opt}$  and  $\alpha$  was not rejected for either  $F_{opt}$  or  $\alpha$ ; NDVI, EVI, and RDVI all  
353 | correlated all with spatial and inter-annual dynamics in  $F_{opt}$  and  $\alpha$  (Table 5). However, it was surprising that NDVI<sub>peak</sub>  
354 | had the strongest correlation with spatial and inter-annual variability for  $F_{opt}$  (Table 5). Both EVI and RDVI should be  
355 | less sensitive to saturation effects than NDVI (Huete et al., 2002; Roujean and Breon, 1995), and based on this it can be  
356 | assumed that peak values of these indices should have stronger relationships to peak values of  $F_{opt}$  and  $\alpha$ . However,  
357 | vegetation indices with a high sensitivity to changes in green biomass at high biomass loads, getsbecome less sensitive  
358 | to green biomass changes at low biomass loads (Huete et al., 2002). The Ppeak leaf area index for ecosystems across the  
359 | Sahel is generally  $\sim 2 \text{ m}^2 \text{ m}^{-2}$  or less, whereas the saturation issue of NDVI generally starts at a leaf area index of about  
360 |  $2\text{-}5 \text{ m}^2 \text{ m}^{-2}$  (Haboudane et al., 2004).

361 | The  $F_{opt\_peak}$  estimates from Agoufou, Demokeya, and the Wankama sites were similar, whereas Dahra and Kelma  
362 | values were high in relation to previously reported canopy-scale  $F_{opt\_peak}$  from the Sahel ( $\sim 8$  to  $\sim 23 \mu\text{mol m}^{-2} \text{ sec}^{-1}$ )  
363 | (Hanan et al., 1998; Merbold et al., 2009; Moncrieff et al., 1997; Boulain et al., 2009; Levy et al., 1997; Monteny et  
364 | al., 1997). These previous studies reported much lower  $F_{opt}$  at canopy scale than at leaf scale (e.g. Levy et al. (1997): 10 vs.

365 | 44  $\mu\text{mol m}^{-2} \text{sec}^{-1}$ ; Boulain et al. (2009): 8 vs. 50  $\mu\text{mol m}^{-2} \text{sec}^{-1}$ . ~~The~~ leaf area index at Dahra and Kelma peaked at  
366 | 2.1 and 2.7, respectively (Timouk et al., 2009; Tagesson et al., 2015a), and it was substantially higher than at the above-  
367 | mentioned sites. A possible explanation ~~to~~for high  $F_{\text{opt}}$  estimates at Dahra and Kelma could there~~fore~~by be the higher  
368 | leaf area index. Tagesson et al. (2016b) performed a quality check of the EC data due to the high net  $\text{CO}_2$  exchange  
369 | measured at the Dahra field site and explained the high values by a combination of moderately dense herbaceous C4  
370 | ground vegetation, high soil nutrient availability, and a grazing pressure resulting in compensatory growth and  
371 | fertilization effects. Another possible explanation could be that the West African Monsoon brings a humid layer of  
372 | surface air from the Atlantic, possibly increasing vegetation production for the most western part of ~~the~~ Sahel (Tagesson  
373 | et al., 2016a).

374 | Our model substantially overestimated GPP for Wankama Millet (Fig. 7f). Being a crop field, this site differed from  
375 | the other sites ~~by~~in its species composition, ~~and~~ ecosystem structure, as well as land and vegetation management. Crop  
376 | fields in southwestern Niger are generally characterized by ~~a~~rather low production, resulting from decreased fertility  
377 | and soil loss caused by intensive land use (Cappelaere et al., 2009). These specifics of the Wankama Millet site may  
378 | cause the model, parameteri~~z~~ed with observations from the other study sites without this strong anthropogenic  
379 | influence, to overestimate GPP at this site. Similar results were found by Boulain et al. (2009) when applying an up-  
380 | scaling model using leaf area index for Wankama Millet and Wankama Fallow. It worked well for Wankama fallow,  
381 | whereas it was less conclusive for Wankama Millet. The main explanation for this difference was low leaf area index in  
382 | millet fields because of a low density of millet stands due to agricultural practice. There is extensive savanna clearing  
383 | for food production in ~~the~~ Sahel (Leblanc et al., 2008; Boulain et al., 2009; Cappelaere et al., 2009). To further  
384 | understand impacts of this land cover change on vegetation production and land-atmosphere exchange processes, ~~it is~~  
385 | ~~of~~there is an urgent need for more study sites covering cropped areas in this region.

386 | In Demokeya, GPP was slightly underestimated for the year 2008 (Fig. 7c) because modelled  $F_{\text{opt}}$  was much lower  
387 | than the actual measured value in 2008 (the thick black line in Fig. 4). An improvement of the model could be to  
388 | incorporate some parameters that constrain or enhance  $F_{\text{opt}}$  depending on environmental stress. Indeed, the regression  
389 | tree analysis indicated that incorporating hydrometeorological variables increased the ability to predict both  $F_{\text{opt}}$  and  $\alpha$ .  
390 | On the other hand, for spatial upscaling purposes, it has been shown that including modelled hydrometeorological  
391 | constraints on LUE decreases the ability to predict vegetation production due to the incorporated uncertainty in these  
392 | modelled variables (Fensholt et al., 2006; Ma et al., 2014). For spatial upscaling to regional scales, it is therefore better  
393 | to simply use relationships to EO data. This is particularly the case for ~~the~~ Sahel, one of the largest dryland areas in the  
394 | world, ~~that~~which includes only a few sites of hydrometeorological observations.

395 | The pattern seen in the spatially explicit GPP budgets (Fig. 5c) may be influenced by a range of biophysical and  
396 | anthropogenic factors. The clear North-South gradient is expected given the strong North-South rainfall gradient in ~~the~~  
397 | Sahel. The West African Monsoon mentioned above could also be an explanation of high GPP values in the western  
398 | part of ~~the~~ Sahel, where values were relatively high in relation to GPP at similar latitudes in the central and eastern  
399 | Sahel (Fig. 5c). The areas with highest GPP are sparsely populated woodlands or shrubby savanna with a relatively  
400 | dense tree cover (Brandt et al., 2016). However, the maps produced should be used with caution as they are based on  
401 | up-scaling of the only six available EC sites that exist in the region; especially given the issues related to the cropped  
402 | fields discussed earlier. Still, the average GPP budget for the entire Sahel 2001-2014 was close to an average annual  
403 | GPP budget as estimated for these six sites ( $692 \pm 89 \text{ g C m}^{-2} \text{ y}^{-1}$ ) (Tagesson et al., 2016a). The range of GPP budgets in

404 Fig. 5c is also similar to previous annual GPP budgets reported from other savanna areas across the world (Veenendaal  
405 et al., 2004; Chen et al., 2003; Kanniah et al., 2010; Chen et al., 2016).

406 Although MOD17A2 GPP has previously been shown to capture GPP in several ecosystems types well (Turner et al.,  
407 2006; Turner et al., 2005; Heinsch et al., 2006; Sims et al., 2006; Kanniah et al., 2009), it has been shown to  
408 underestimate it for others (Coops et al., 2007; Gebremichael and Barros, 2006; Sjöström et al., 2013). GPP of Sahelian  
409 drylands have not been captured well by MOD17A2 ~~well~~ (Sjöström et al., 2013; Fensholt et al., 2006), and as we have  
410 shown, this underestimation persists in the latest MOD17A2H GPP (collection 6) product (Fig. 2). The main reason for  
411 this pronounced underestimation is that maximum LUE is set to 0.84 g C MJ<sup>-1</sup> (open shrubland; Demokeya) and 0.86 g  
412 C MJ<sup>-1</sup> (grassland; Agoufou, Dahra, Kelma; Wankama Millet and Wankama Fallow) in the BPLUT, i.e. much lower  
413 than maximum LUE measured at the Sahelian measurement sites of this study (average: 2.47 g C MJ<sup>-1</sup>; range: 1.58-3.50  
414 g C MJ<sup>-1</sup>) (Sjöström et al., 2013; Tagesson et al., 2015a), a global estimate of ~1.5 g C MJ<sup>-1</sup> (Garbulsy et al., 2010),  
415 and a savanna site in Australia (1.26 g C MJ<sup>-1</sup>) (Kanniah et al., 2009).

416 Several dynamic global vegetation models have been used for decades to quantify GPP at different spatial and  
417 temporal scales (Dickinson, 1983; Sellers et al., 1997). These models are generally based on the photosynthesis model  
418 of Farquhar et al. (1980), a model particularly sensitive to uncertainty in photosynthetic capacity (Zhang et al., 2014).  
419 This and several previous studies have shown that both photosynthetic capacity and efficiency (both  $\alpha$  and LUE) can  
420 vary considerably between seasons as well as spatially, and both within and between vegetation types (Eamus et al.,  
421 2013; Garbulsy et al., 2010; Ma et al., 2014; Tagesson et al., 2015a). This variability is difficult to estimate using  
422 broad values based on land cover classes, yet most models apply a constant value, which can cause substantial  
423 inaccuracies in the estimates of seasonal and spatial variability in GPP. This is particularly a problem in savannas that  
424 consists of several plant functional types (C3 and C4 species, and a large variability in tree/herbaceous vegetation  
425 fractions) (Scholes and Archer, 1997). This study indicates the strong applicability of EO as a tool for parameterizing  
426 spatially explicit estimates of plant physiological variables, which could improve our ability to simulate GPP. Spatially  
427 explicit estimates of GPP at a high temporal and spatial resolution are essential for environmental change studies in the  
428 Sahel and can contribute to increased knowledge regarding changes in GPP, its relationship to climatic change and  
429 anthropogenic forcing, and estimations of ecosystem processes and biochemical and hydrological cycles.

430  
431 **Acknowledgements** Data is available from Fluxnet (<http://fluxnet.ornl.gov>) and CarboAfrica  
432 ([http://www.carboafrica.net/index\\_en.asp](http://www.carboafrica.net/index_en.asp)). Data for the Mali and Niger sites were made available by the AMMA-  
433 CATCH regional observatory ([www.amma-catch.org](http://www.amma-catch.org)), which is funded by the French Institut de Recherche pour le  
434 Développement (IRD) and Institut National des Sciences de l'Univers (INSU). The project was funded by the Danish  
435 Council for Independent Research (DFF) Sapere Aude programme. The Faculty of Science, Lund University supported  
436 the Dahra and Demokeya measurements with an infrastructure grant. Ardö received support from the Swedish National  
437 Space Board.

438  
439 **References**  
440 Abdi, A., Seaquist, J., Tenenbaum, D., Eklundh, L., and Ardö, J.: The supply and demand of net  
441 primary production in the Sahel, *Environ. Res. Lett.*, 9, 094003, doi:10.1088/1748-9326/9/9/094003,  
442 2014.

443 Ahlström, A., Raupach, M. R., Schurgers, G., Smith, B., Arneth, A., Jung, M., Reichstein, M.,  
444 Canadell, J. G., Friedlingstein, P., Jain, A. K., Kato, E., Poulter, B., Sitch, S., Stocker, B. D., Viovy,  
445 N., Wang, Y. P., Wiltshire, A., Zaehle, S., and Zeng, N.: The dominant role of semi-arid ecosystems  
446 in the trend and variability of the land CO<sub>2</sub> sink, *Science*, 348, 895-899, 10.1126/science.aaa1668,  
447 2015.

448 Baldocchi, D., Falge, E., Gu, L., Olson, R., Hollinger, D., Running, S., Anthoni, P., Bernhofer, C.,  
449 Davis, K., Evans, R., Fuentes, J., Goldstein, A., Katul, G., Law, B., Lee, X., Malhi, Y., Meyers, T.,  
450 Munger, W., Oechel, W., Paw, K. T., Pilegaard, K., Schmid, H. P., Valentini, R., Verma, S., Vesala,  
451 T., Wilson, K., and Wofsy, S.: FLUXNET: A New Tool to Study the Temporal and Spatial  
452 Variability of Ecosystem-Scale Carbon Dioxide, Water Vapor, and Energy Flux Densities, *Bull.*  
453 *Am. Meteorol. Soc.*, 82, 2415-2434, 10.1175/1520-0477(2001)082<2415:fanfts>2.3.co;2, 2001.

454 Boulain, N., Cappelaere, B., Ramier, D., Issoufou, H. B. A., Halilou, O., Seghieri, J., Guillemain, F.,  
455 Oï, M., Gignoux, J., and Timouk, F.: Towards an understanding of coupled physical and biological  
456 processes in the cultivated Sahel – 2. Vegetation and carbon dynamics, *J. Hydrol.*, 375, 190-203,  
457 10.1016/j.jhydrol.2008.11.045, 2009.

458 Brandt, M., Hiernaux, P., Rasmussen, K., Mbow, C., Kergoat, L., Tagesson, T., Ibrahim, Y. Z.,  
459 Wélé, A., Tucker, C. J., and Fensholt, R.: Assessing woody vegetation trends in Sahelian drylands  
460 using MODIS based seasonal metrics, *Remote Sens. Environ.*, 183, 215-  
461 225, <http://dx.doi.org/10.1016/j.rse.2016.05.027>, 2016.

462 Broge, N. H., and Leblanc, E.: Comparing prediction power and stability of broadband and  
463 hyperspectral vegetation indices for estimation of green leaf area index and canopy chlorophyll  
464 density, *Remote Sens. Environ.*, 76, 156-172, [http://dx.doi.org/10.1016/S0034-4257\(00\)00197-8](http://dx.doi.org/10.1016/S0034-4257(00)00197-8),  
465 2001.

466 Cannell, M., and Thornley, J.: Temperature and CO<sub>2</sub> Responses of Leaf and Canopy Photosynthesis:  
467 a Clarification using the Non-rectangular Hyperbola Model of Photosynthesis, *Ann. Bot.*, 82, 883-  
468 892, 1998.

469 Cappelaere, B., Descroix, L., Lebel, T., Boulain, N., Ramier, D., Laurent, J. P., Favreau, G.,  
470 Boubkraoui, S., Boucher, M., Bouzou Moussa, I., Chaffard, V., Hiernaux, P., Issoufou, H. B. A., Le  
471 Breton, E., Mamadou, I., Nazoumou, Y., Oï, M., Otlé, C., and Quantin, G.: The AMMA-CATCH  
472 experiment in the cultivated Sahelian area of south-west Niger – Investigating water cycle response  
473 to a fluctuating climate and changing environment, *J. Hydrol.*, 375, 34-51,  
474 10.1016/j.jhydrol.2009.06.021, 2009.

475 Chen, C., Cleverly, J., and Zhang, L.: Modelling Seasonal and Inter-annual Variations in Carbon  
476 and Water Fluxes in an Arid-Zone Acacia Savanna Woodland, 1981–2012, *Ecosystems*, 19, 625-  
477 644, 2016.

478 Chen, X., Hutley, L., and Eamus, D.: Carbon balance of a tropical savanna of northern Australia.,  
479 *Oecologia*, 137, 405-416, 2003.

480 Coops, N. C., Black, T. A., Jassal, R. S., Trofymow, J. A., and Morgenstern, K.: Comparison of  
481 MODIS, eddy covariance determined and physiologically modelled gross primary production (GPP)  
482 in a Douglas-fir forest stand, *Remote Sens. Environ.*, 107, 385-  
483 401, <http://dx.doi.org/10.1016/j.rse.2006.09.010>, 2007.

484 Dardel, C., Kergoat, L., Hiernaux, P., Mougin, E., Grippa, M., and Tucker, C. J.: Re-greening Sahel:  
485 30 years of remote sensing data and field observations (Mali, Niger), *Remote Sens. Environ.*, 140,  
486 350-364, <http://dx.doi.org/10.1016/j.rse.2013.09.011>, 2014.

487 De'ath, G., and Fabricius, K. E.: Classification and regression trees: A powerful yet simple  
488 technique for ecological data analysis, *Ecology*, 81, 3178-3192, 10.2307/177409, 2000.

Field Code Changed

Field Code Changed

Field Code Changed

Field Code Changed

489 de Ridder, N., Stroosnijder, L., and Cisse, A. M.: Productivity of Sahelian rangelands : a study of  
490 the soils, the vegetations and the exploitation of that natural resource, PPS course book. Primary  
491 Production in the Sahel, Agricultural University, Wageningen, 1982.

492 Dee, D. P., Uppala, S. M., Simmons, A. J., Berrisford, P., Poli, P., Kobayashi, S., Andrae, U.,  
493 Balmaseda, M. A., Balsamo, G., Bauer, P., Bechtold, P., Beljaars, A. C. M., van de Berg, L., Bidlot,  
494 J., Bormann, N., Delsol, C., Dragani, R., Fuentes, M., Geer, A. J., Haimberger, L., Healy, S. B.,  
495 Hersbach, H., Hólm, E. V., Isaksen, I., Kållberg, P., Köhler, M., Matricardi, M., McNally, A. P.,  
496 Monge-Sanz, B. M., Morcrette, J. J., Park, B. K., Peubey, C., de Rosnay, P., Tavolato, C., Thépaut,  
497 J. N., and Vitart, F.: The ERA-Interim reanalysis: configuration and performance of the data  
498 assimilation system, *Q. J. Roy. Meteor. Soc.*, 137, 553-597, 10.1002/qj.828, 2011.

499 Dickinson, R. E.: Land Surface Processes and Climate—Surface Albedos and Energy Balance, in:  
500 *Advances in Geophysics*, edited by: Barry, S., Elsevier, 305-353, 1983.

501 Eamus, D., Cleverly, J., Boulain, N., Grant, N., Faux, R., and Villalobos-Vega, R.: Carbon and  
502 water fluxes in an arid-zone *Acacia* savanna woodland: An analyses of seasonal patterns and  
503 responses to rainfall events, *Agric. For. Meteorol.*, 182–183, 225-  
504 238, <http://dx.doi.org/10.1016/j.agrformet.2013.04.020>, 2013.

505 ECMWF: ERA Interim Daily: <http://apps.ecmwf.int/datasets/data/interim-full-daily/levtype=sfc/>,  
506 access: 04-04-2016, 2016a.

507 ECMWF: ERA-Interim: surface photosynthetically active radiation (surface PAR) values are too  
508 low [https://software.ecmwf.int/wiki/display/CKB/ERA-  
509 Interim%3A+surface+photosynthetically+active+radiation+%28surface+PAR%29+values+are+too  
510 +low](https://software.ecmwf.int/wiki/display/CKB/ERA-Interim%3A+surface+photosynthetically+active+radiation+%28surface+PAR%29+values+are+too+low), access: 7 November, 2016b.

511 Falge, E., Baldocchi, D., Olson, R., Anthoni, P., Aubinet, M., Bernhofer, C., Burba, G., Ceulemans,  
512 R., Clement, R., Dolman, H., Granier, A., Gross, P., Grunwald, T., Hollinger, D., Jensen, N. O.,  
513 Katul, G., Keronen, P., Kowalski, A., Lai, C. T., Law, B. E., Meyers, T., Moncrieff, J. B., Moors, E.,  
514 Munger, J. W., Pilegaard, K., Rannik, U., Rebmann, C., Suyker, A., Tenhunen, J., Tu, K., Verma,  
515 S., Vesala, T., Wilson, K., and Wofsy, S.: Gap filling strategies for defensible annual sums of net  
516 ecosystem exchange, *Agric. For. Meteorol.*, 107, 43-69, 2001.

517 Farquhar, G. D., Caemmerer, S., and Berry, J. A.: A biochemical model of photosynthetic CO<sub>2</sub>  
518 assimilation in leaves of C3 plants, *Planta*, 149, 78-90, 1980.

519 Fensholt, R., and Sandholt, I.: Derivation of a shortwave infrared water stress index from MODIS  
520 near- and shortwave infrared data in a semiarid environment, *Remote Sens. Environ.*, 87, 111-  
521 121, <http://dx.doi.org/10.1016/j.rse.2003.07.002>, 2003.

522 Fensholt, R., Sandholt, I., Rasmussen, M. S., Stisen, S., and Diouf, A.: Evaluation of satellite based  
523 primary production modelling in the semi-arid Sahel, *Remote Sens. Environ.*, 105, 173-188,  
524 10.1016/j.rse.2006.06.011, 2006.

525 Fensholt, R., Rasmussen, K., Kaspersen, P., Huber, S., Horion, S., and Swinnen, E.: Assessing Land  
526 Degradation/Recovery in the African Sahel from Long-Term Earth Observation Based Primary  
527 Productivity and Precipitation Relationships, *Remote Sensing*, 5, 664-686, 2013.

528 Garbulsky, M. F., Peñuelas, J., Papale, D., Ardö, J., Goulden, M. L., Kiely, G., Richardson, A. D.,  
529 Rotenberg, E., Veenendaal, E. M., and Filella, I.: Patterns and controls of the variability of radiation  
530 use efficiency and primary productivity across terrestrial ecosystems, *Global Ecol. Biogeogr.*, 19,  
531 253-267, 10.1111/j.1466-8238.2009.00504.x, 2010.

532 Gates, D. M., Keegan, H. J., Schleter, J. C., and Weidner, V. R.: Spectral Properties of Plants, *Appl.*  
533 *Optics*, 4, 11-20, 1965.

534 Gebremichael, M., and Barros, A. P.: Evaluation of MODIS Gross Primary Productivity (GPP) in  
535 tropical monsoon regions, *Remote Sens. Environ.*, 100, 150-  
536 166, <http://dx.doi.org/10.1016/j.rse.2005.10.009>, 2006.

Field Code Changed

Field Code Changed

Field Code Changed

Field Code Changed

Field Code Changed

537 Haboudane, D., Miller, J. R., Pattey, E., Zarco-Tejada, P. J., and Strachan, I. B.: Hyperspectral  
538 vegetation indices and novel algorithms for predicting green LAI of crop canopies: Modeling and  
539 validation in the context of precision agriculture, *Remote Sens. Environ.*, 90, 337-  
540 352, <http://dx.doi.org/10.1016/j.rse.2003.12.013>, 2004.

541 Hanan, N., Kabat, P., Dolman, J., and Elbers, J. A. N.: Photosynthesis and carbon balance of a  
542 Sahelian fallow savanna, *Global Change Biol.*, 4, 523-538, 1998.

543 Heinsch, F. A., Maosheng, Z., Running, S. W., Kimball, J. S., Nemani, R. R., Davis, K. J., Bolstad,  
544 P. V., Cook, B. D., Desai, A. R., Ricciuto, D. M., Law, B. E., Oechel, W. C., Hyojung, K., Hongyan,  
545 L., Wofsy, S. C., Dunn, A. L., Munger, J. W., Baldocchi, D. D., Liukang, X., Hollinger, D. Y.,  
546 Richardson, A. D., Stoy, P. C., Siqueira, M. B. S., Monson, R. K., Burns, S. P., and Flanagan, L. B.:  
547 Evaluation of remote sensing based terrestrial productivity from MODIS using regional tower eddy  
548 flux network observations, *IEEE T. Geosci. Remote*, 44, 1908-1925, 10.1109/TGRS.2005.853936,  
549 2006.

550 Hickler, T., Eklundh, L., Seaquist, J. W., Smith, B., Ardö, J., Olsson, L., Sykes, M. T., and  
551 Sjöström, M.: Precipitation controls Sahel greening trend, *Geophys. Res. Lett.*, 32, L21415,  
552 doi:10.1029/2005GL024370, 2005.

553 Huber, S., Tagesson, T., and Fensholt, R.: An automated field spectrometer system for studying  
554 VIS, NIR and SWIR anisotropy for semi-arid savanna, *Remote Sens. Environ.*, 152, 547–556, 2014.

555 Huete, A., Didan, K., Miura, T., Rodriguez, E. P., Gao, X., and Ferreira, L. G.: Overview of the  
556 radiometric and biophysical performance of the MODIS vegetation indices, *Remote Sens. Environ.*,  
557 83, 195–213, 2002.

558 Ide, R., Nakaji, T., and Oguma, H.: Assessment of canopy photosynthetic capacity and estimation  
559 of GPP by using spectral vegetation indices and the light-response function in a larch forest, *Agric.*  
560 *For. Meteorol.*, 150, 389-398, 2010.

561 Inoue, Y., Penuelas, J., Miyata, A., and Mano, M.: Normalized difference spectral indices for  
562 estimating photosynthetic efficiency and capacity at a canopy scale derived from hyperspectral and  
563 CO<sub>2</sub> flux measurements in rice, *Remote Sens. Environ.*, 112, 156-172, 2008.

564 Jin, H., and Eklundh, L.: A physically based vegetation index for improved monitoring of plant  
565 phenology, *Remote Sens. Environ.*, 152, 512-525, <http://dx.doi.org/10.1016/j.rse.2014.07.010>, 2014.

566 Kanniah, K. D., Beringer, J., Hutley, L. B., Tapper, N. J., and Zhu, X.: Evaluation of Collections 4  
567 and 5 of the MODIS Gross Primary Productivity product and algorithm improvement at a tropical  
568 savanna site in northern Australia, *Remote Sens. Environ.*, 113, 1808-  
569 1822, <http://dx.doi.org/10.1016/j.rse.2009.04.013>, 2009.

570 Kanniah, K. D., Beringer, J., and Hutley, L. B.: The comparative role of key environmental factors  
571 in determining savanna productivity and carbon fluxes: A review, with special reference to  
572 Northern Australia, *Progress in Physical Geography*, 34, 459-490, 2010.

573 Kergoat, L., Lafont, S., Arneth, A., Le Dantec, V., and Saugier, B.: Nitrogen controls plant canopy  
574 light-use efficiency in temperate and boreal ecosystems, *J. Geophys. Res.*, 113, 1-19,  
575 10.1029/2007JG000676, 2008.

576 Leblanc, M. J., Favreau, G., Massuel, S., Tweed, S. O., Loireau, M., and Cappelaere, B.: Land  
577 clearance and hydrological change in the Sahel: SW Niger, *Global Planet. Change*, 61, 135-  
578 150, <http://dx.doi.org/10.1016/j.gloplacha.2007.08.011>, 2008.

579 Levy, P. E., Moncrieff, J. B., Massheder, J. M., Jarvis, P. G., Scott, S. L., and Brouwer, J.: CO<sub>2</sub>  
580 fluxes at leaf and canopy scale in millet, fallow and tiger bush vegetation at the HAPEX-Sahel  
581 southern super-site, *J. Hydrol.*, 188, 612-632, [http://dx.doi.org/10.1016/S0022-1694\(96\)03195-2](http://dx.doi.org/10.1016/S0022-1694(96)03195-2),  
582 1997.

583 Ma, X., Huete, A., Yu, Q., Restrepo-Coupe, N., Beringer, J., Hutley, L. B., Kanniah, K. D.,  
584 Cleverly, J., and Eamus, D.: Parameterization of an ecosystem light-use-efficiency model for

Field Code Changed

Field Code Changed

Field Code Changed

Field Code Changed

Field Code Changed



585 predicting savanna GPP using MODIS EVI, *Remote Sens. Environ.*, 154, 253-  
586 271, <http://dx.doi.org/10.1016/j.rse.2014.08.025>, 2014.

587 Mayaux, P., Bartholomé, E., Massart, M., Cutsem, C. V., Cabral, A., Nonguierma, A., Diallo, O.,  
588 Pretorius, C., Thompson, M., Cherlet, M., Pekel, J.-F., Defourny, P., Vasconcelos, M., Gregorio, A.  
589 D., S.Fritz, Grandi, G. D., C.Elvidge, P.Vogt, and Belward, A.: EUR 20665 EN –A Land-cover  
590 map of Africa, edited by: Centre', E. C. J. R., European Commissions Joint Research Centre,  
591 Luxembourg, 38 pp., 2003.

592 Mbow, C., Fensholt, R., Rasmussen, K., and Diop, D.: Can vegetation productivity be derived from  
593 greenness in a semi-arid environment? Evidence from ground-based measurements, *J. Arid*  
594 *Environ.*, 97, 56-65, <http://dx.doi.org/10.1016/j.jaridenv.2013.05.011>, 2013.

595 Merbold, L., Ardö, J., Arneth, A., Scholes, R. J., Nouvellon, Y., de Grandcourt, A., Archibald, S.,  
596 Bonnefond, J. M., Boulain, N., Brueggemann, N., Bruemmer, C., Cappelaere, B., Ceschia, E., El-  
597 Khidir, H. A. M., El-Tahir, B. A., Falk, U., Lloyd, J., Kergoat, L., Le Dantec, V., Mougín, E.,  
598 Muchinda, M., Mukelabai, M. M., Ramier, D., Rouspard, O., Timouk, F., Veenendaal, E. M., and  
599 Kutsch, W. L.: Precipitation as driver of carbon fluxes in 11 African ecosystems, *Biogeosciences*, 6,  
600 1027-1041, 10.5194/bg-6-1027-2009, 2009.

601 Moncrieff, J. B., Monteny, B., Verhoef, A., Friborg, T., Elbers, J., Kabat, P., de Bruin, H., Soegaard,  
602 H., Jarvis, P. G., and Taupin, J. D.: Spatial and temporal variations in net carbon flux during  
603 HAPEX-Sahel, *J. Hydrol.*, 188–189, 563-588, 10.1016/s0022-1694(96)03193-9, 1997.

604 Monteith, J. L.: Solar radiation and productivity in tropical ecosystems, *J. Appl. Ecol.*, 9, 747-766,  
605 1972.

606 Monteith, J. L.: Climate and the efficiency of crop production in Britain, *Philos. Trans. Roy. Soc. B.*,  
607 281, 277-294, 1977.

608 Monteny, B. A., Lhomme, J. P., Chehbouni, A., Troufleau, D., Amadou, M., Sicot, M., Verhoef, A.,  
609 Galle, S., Said, F., and Lloyd, C. R.: The role of the Sahelian biosphere on the water and the CO2  
610 cycle during the HAPEX-Sahel experiment, *J. Hydrol.*, 188, 516-  
611 535, [http://dx.doi.org/10.1016/S0022-1694\(96\)03191-5](http://dx.doi.org/10.1016/S0022-1694(96)03191-5), 1997.

612 Mutanga, O., and Skidmore, A. K.: Narrow band vegetation indices overcome the saturation  
613 problem in biomass estimation, *Int. J. Remote Sens.*, 25, 3999-4014,  
614 10.1080/01431160310001654923, 2004.

615 NASA: Reverb ECHO: <http://reverb.echo.nasa.gov/reverb/>, access: June 2016, 2016.

616 Papale, D., Reichstein, M., Aubinet, M., Canfora, E., Bernhofer, C., Kutsch, W., Longdoz, B.,  
617 Rambal, S., Valentini, R., Vesala, T., and Yakir, D.: Towards a standardized processing of Net  
618 Ecosystem Exchange measured with eddy covariance technique: algorithms and uncertainty  
619 estimation, *Biogeosciences*, 3, 571-583, 10.5194/bg-3-571-2006, 2006.

620 Paruelo, J. M., Garbulsky, M. F., Guerschman, J. P., and Jobbágy, E. G.: Two decades of  
621 Normalized Difference Vegetation Index changes in South America: identifying the imprint of  
622 global change, *Int. J. Remote Sens.*, 25, 2793-2806, 10.1080/01431160310001619526, 2004.

623 Poulter, B., Frank, D., Ciais, P., Myneni, R. B., Andela, N., Bi, J., Broquet, G., Canadell, J. G.,  
624 Chevallier, F., Liu, Y. Y., Running, S. W., Sitch, S., and van der Werf, G. R.: Contribution of semi-  
625 arid ecosystems to interannual variability of the global carbon cycle, *Nature*, 509, 600-603,  
626 10.1038/nature13376, 2014.

627 Prince, S. D., Kerr, Y. H., Goutorbe, J. P., Lebel, T., Tinga, A., Bessemoulin, P., Brouwer, J.,  
628 Dolman, A. J., Engman, E. T., Gash, J. H. C., Hoepffner, M., Kabat, P., Monteny, B., Said, F.,  
629 Sellers, P., and Wallace, J.: Geographical, biological and remote sensing aspects of the hydrologic  
630 atmospheric pilot experiment in the sahel (HAPEX-Sahel), *Remote Sens. Environ.*, 51, 215-  
631 234, [http://dx.doi.org/10.1016/0034-4257\(94\)00076-Y](http://dx.doi.org/10.1016/0034-4257(94)00076-Y), 1995.

Field Code Changed

Field Code Changed

Field Code Changed

Field Code Changed

Field Code Changed

632 Qi, J., Chehbouni, A., Huete, A. R., Kerr, Y. H., and Sorooshian, S.: A modified soil adjusted  
633 vegetation index, *Remote Sens. Environ.*, 48, 119-126, 1994.

634 Richter, K., Atzberger, C., Hank, T. B., and Mauser, W.: Derivation of biophysical variables from  
635 Earth observation data: validation and statistical measures, *J. Appl. Remote Sens.*, 6, 063557,  
636 10.1117/1.JRS.6.063557, 2012.

637 Rietkerk, M., Ketner, P., Stroosnijder, L., and Prins, H. H. T.: Sahelian rangeland development; a  
638 catastrophe?, *J. Range Manage.*, 49, 512-519, 1996.

639 Rockström, J., and de Rouw, A.: Water, nutrients and slope position in on-farm pearl millet  
640 cultivation in the Sahel, *Plant Soil*, 195, 311-327, 10.1023/A:1004233303066, 1997.

641 Roujean, J.-L., and Breon, F.-M.: Estimating PAR absorbed by vegetation from bidirectional  
642 reflectance measurements, *Remote Sens. Environ.*, 51, 375-384, [http://dx.doi.org/10.1016/0034-  
643 4257\(94\)00114-3](http://dx.doi.org/10.1016/0034-4257(94)00114-3), 1995.

644 Rouse, J. W., Haas, R. H., Schell, J. A., Deering, D. W., and Harlan, J. C.: Monitoring the Vernal  
645 Advancement of Retrogradation of Natural Vegetation, Type III, Final Report, Greenbelt, MD,  
646 1974.

647 Ruimy, A., Saugier, B., and Dedieu, G.: Methodology for the estimation of terrestrial net primary  
648 production from remotely sensed data., *J. Geophys. Res.*, 99, 5263-5283., 1994.

649 Running, S. W., Nemani, R. R., Heinsch, F. A., Zhao, M., Reeves, M., and Hashimoto, H.: A  
650 Continuous Satellite-Derived Measure of Global Terrestrial Primary Production, *BioScience*, 54,  
651 547-560, 10.1641/0006-3568(2004)054[0547:ACSMOG]2.0.CO;2, 2004.

652 Running, S. W., and Zhao, M.: User's Guide. Daily GPP and Annual NPP (MOD17A2/A3)  
653 Products NASA Earth Observing System MODIS Land Algorithm. Version 3.0 For Collection 6.,  
654 University of Montana, USA, NASA, 2015.

655 Scholes, R. J., and Archer, S. R.: Tree-grass interactions in savannas, *Annual Review of Ecology  
656 and Systematics*, 28, 517-544, 1997.

657 Sellers, P. J., Dickinson, R. E., Randall, D. A., Betts, A. K., Hall, F. G., Berry, J. A., Collatz, G. J.,  
658 Denning, A. S., Mooney, H. A., Nobre, C. A., Sato, N., Field, C. B., and Henderson-Sellers, A.:  
659 Modeling the Exchanges of Energy, Water, and Carbon Between Continents and the Atmosphere,  
660 *Science*, 275, 502-509, 10.1126/science.275.5299.502, 1997.

661 Sims, D. A., Rahman, A. F., Cordova, V. D., El-Masri, B. Z., Baldocchi, D. D., Flanagan, L. B.,  
662 Goldstein, A. H., Hollinger, D. Y., Misson, L., Monson, R. K., Oechel, W. C., Schmid, H. P.,  
663 Wofsy, S. C., and Xu, L.: On the use of MODIS EVI to assess gross primary productivity of North  
664 American ecosystems, *J. Geophys. Res.*, 111, G04015, 10.1029/2006JG000162, 2006.

665 Sjöström, M., Ardö, J., Eklundh, L., El-Tahir, B. A., El-Khidir, H. A. M., Hellström, M., Pilesjö, P.,  
666 and Seaquist, J.: Evaluation of satellite based indices for gross primary production estimates in a  
667 sparse savanna in the Sudan, *Biogeosciences*, 6, 129-138, 2009.

668 Sjöström, M., Zhao, M., Archibald, S., Arneth, A., Cappelaere, B., Falk, U., de Grandcourt, A.,  
669 Hanan, N., Kergoat, L., Kutsch, W., Merbold, L., Mougou, E., Nickless, A., Nouvellon, Y., Scholes,  
670 R. J., Veenendaal, E. M., and Ardö, J.: Evaluation of MODIS gross primary productivity for Africa  
671 using eddy covariance data, *Remote Sens. Environ.*, 131, 275-  
672 286, <http://dx.doi.org/10.1016/j.rse.2012.12.023>, 2013.

673 Tagesson, T., Eklundh, L., and Lindroth, A.: Applicability of leaf area index products for boreal  
674 regions of Sweden, *Int. J. Remote Sens.*, 30, 5619-5632, 2009.

675 Tagesson, T., Fensholt, R., Cropley, F., Guiro, I., Horion, S., Ehammer, A., and Ardö, J.: Dynamics  
676 in carbon exchange fluxes for a grazed semi-arid savanna ecosystem in West Africa, *Agr. Ecosyst.  
677 Environ.*, 205, 15-24, <http://dx.doi.org/10.1016/j.agee.2015.02.017>, 2015a.

678 Tagesson, T., Fensholt, R., Guiro, I., Rasmussen, M. O., Huber, S., Mbow, C., Garcia, M., Horion,  
679 S., Sandholt, I., Rasmussen, B. H., Götsche, F. M., Ridler, M.-E., Olén, N., Olsen, J. L., Ehammer,

Field Code Changed

Field Code Changed

Field Code Changed

680 A., Madsen, M., Olesen, F. S., and Ardö, J.: Ecosystem properties of semi-arid savanna grassland in  
681 West Africa and its relationship to environmental variability, *Global Change Biol.*, 21, 250-264, doi:  
682 10.1111/gcb.12734, 2015b.

683 Tagesson, T., Fensholt, R., Huber, S., Horion, S., Guiro, I., Ehammer, A., and Ardö, J.: Deriving  
684 seasonal dynamics in ecosystem properties of semi-arid savannas using in situ based hyperspectral  
685 reflectance, *Biogeosciences*, 12, 4621-4635, doi:10.5194/bg-12-4621-2015, 2015c.

686 Tagesson, T., Fensholt, R., Cappelare, B., E., M., Horion, S., L., K., Nieto, H., Ehammer, A.,  
687 Demarty, J., and Ardö, J.: Spatiotemporal variability in carbon exchange fluxes across the Sahel  
688 *Agric. For. Meteorol.*, 226–227, 108-118, 2016a.

689 Tagesson, T., Fensholt, R., Guiro, I., Cropley, F., Horion, S., Ehammer, A., and Ardö, J.: Very high  
690 carbon exchange fluxes for a grazed semi-arid savanna ecosystem in West Africa, *Danish Journal of*  
691 *Geography*, 116, 93-109, <http://dx.doi.org/10.1080/00167223.2016.1178072>, 2016b.

692 Timouk, F., Kergoat, L., Mougou, E., Lloyd, C. R., Ceschia, E., Cohard, J. M., Rosnay, P. d.,  
693 Hiernaux, P., Demarez, V., and Taylor, C. M.: Response of surface energy balance to water regime  
694 and vegetation development in a Sahelian landscape, *J. Hydrol.*, 375, 12-12,  
695 10.1016/j.jhydrol.2009.04.022, 2009.

696 Turner, D. P., Ritts, W. D., Cohen, W. B., Maeirsperger, T. K., Gower, S. T., Kirschbaum, A. A.,  
697 Running, S. W., Zhao, M., Wofsy, S. C., Dunn, A. L., Law, B. E., Campbell, J. L., Oechel, W. C.,  
698 Kwon, H. J., Meyers, T. P., Small, E. E., Kurc, S. A., and Gamon, J. A.: Site-level evaluation of  
699 satellite-based global terrestrial gross primary production and net primary production monitoring,  
700 *Global Change Biol.*, 11, 666-684, 2005.

701 Turner, D. P., Ritts, W. D., and Cohen, W. B.: Evaluation of MODIS NPP and GPP products across  
702 multiple biomes, *Remote Sens. Environ.*, 102, 282-293, 2006.

703 United Nations: Sahel Regional Strategy Mid-Year Review 2013 New York, 1-59, 2013.

704 Veenendaal, E. M., Kolle, O., and Lloyd, J.: Seasonal variation in energy fluxes and carbon dioxide  
705 exchange for a broadleaved semi-arid savanna (Mopane woodland) in Southern Africa, *Global*  
706 *Change Biol.*, 10, 318-328, 2004.

707 Velluet, C., Demarty, J., Cappelare, B., Braud, I., Issoufou, H. B. A., Boulain, N., Ramier, D.,  
708 Mainassara, I., Charvet, G., Boucher, M., Chazarin, J. P., Oi, M., Yahou, H., Maidaji, B., Arpin-  
709 Pont, F., Benarrosh, N., Mahamane, A., Nazoumou, Y., Favreau, G., and Seghieri, J.: Building a  
710 field- and model-based climatology of local water and energy cycles in the cultivated Sahel; annual  
711 budgets and seasonality, *Hydrol. Earth Syst. Sci.*, 18, 5001-5024, 10.5194/hess-18-5001-2014, 2014.

712 Yoder, B. J., and Pettigrew-Crosby, R. E.: Predicting nitrogen and chlorophyll content and  
713 concentrations from reflectance spectra (400–2500 nm) at leaf and canopy scales, *Remote Sens.*  
714 *Environ.*, 53, 199-211, [http://dx.doi.org/10.1016/0034-4257\(95\)00135-N](http://dx.doi.org/10.1016/0034-4257(95)00135-N), 1995.

715 Zhang, Y., Guanter, L., Berry, J. A., Joiner, J., van der Tol, C., Huete, A., Gitelson, A., Voigt, M.,  
716 and Köhler, P.: Estimation of vegetation photosynthetic capacity from space-based measurements  
717 of chlorophyll fluorescence for terrestrial biosphere models, *Global Change Biol.*, 20, 3727-3742,  
718 10.1111/gcb.12664, 2014.

Formatted: English (U.S.)

Formatted: English (U.S.)

Field Code Changed

Formatted: English (U.S.)

Field Code Changed

Formatted: English (U.S.)

Formatted: English (U.S.)

719  
720

721 **Tables**

722 **Table 1.** Description of the six measurement sites including location, soil type, ecosystem type and dominant species.

Measurement site	Coordinates	Soil type	Ecosystem	Dominant species
Agoufou <sup>a</sup> (ML-AgG, Mali)	15.34°N, 1.48°W	Sandy ferruginous Arenosol	Open woody savannah (4% tree cover)	Trees: <i>Acacia spp.</i> , <i>Balanites aegyptiaca</i> , <i>Combretum glutinosum</i> Herbs: <i>Zornia glochidiata</i> , <i>Cenchrus biflorus</i> , <i>Aristida mutabilis</i> , <i>Tragus berteronianus</i>
Dahra <sup>b</sup> (SN-Dah, Senegal)	15.40°N, 15.43°W	Sandy luvic arenosol	Grassland/shrubland Savanna (3% tree cover)	Trees: <i>Acacia spp.</i> , <i>Balanites aegyptiaca</i> Herbs: <i>Zornia latifolia</i> , <i>Aristida adscensionis</i> , <i>Cenchrus biflorus</i>
Demokeya <sup>c</sup> (SD-Dem, Sudan)	13.28°N, 30.48°E	Cambic Arenosol	Sparse acacia savannah (7% tree cover)	Trees: <i>Acacia spp.</i> , Herbs: <i>Aristida pallida</i> , <i>Eragrostis tremula</i> , <i>Cenchrus biflorus</i>
Kelma <sup>a</sup> (ML-Kem, Mali)	15.22°N, 1.57°W	Clay soil depression	Open acacia forest (90% tree cover)	Trees: <i>Acacia seyal</i> , <i>Acacia nilotica</i> , <i>Balanites aegyptiaca</i> Herbs: <i>Sporobolus hevolvus</i> , <i>Echinochloa colona</i> , <i>Aeschynomene sensitiva</i> <i>Guiera senegalensis</i>
Wankama Fallow <sup>d</sup> (NE-WaF, Niger)	13.65°N, 2.63°E	Sandy ferruginous Arenosol	Fallow bush	
Wankama Millet <sup>e</sup> (NE-WaM, Niger)	13.64°N, 2.63°E	Sandy ferruginous Arenosol	Millet crop	<i>Pennisetum glaucum</i>

723 <sup>a</sup>(Timouk et al., 2009)

724 <sup>b</sup>(Tagesson et al., 2015b)

725 <sup>c</sup>(Sjöström et al., 2009)

726 <sup>d</sup>(Velluet et al., 2014)

727 <sup>e</sup>(Boulain et al., 2009)

Formatted: Danish

Formatted: Danish

Field Code Changed

Formatted: Danish

Formatted: Danish

Field Code Changed

Formatted: Danish

Formatted: Danish

Formatted: Danish

Field Code Changed

Formatted: Danish

Formatted: Danish

**Table 2.** Correlation between intra-annual dynamics in photosynthetic capacity ( $F_{opt}$ ;  $F_{opt\_frac}$  for all sites), quantum efficiency ( $\alpha$ ;  $\alpha_{frac}$  for all sites), and the different vegetation indices for the six measurement sites (Fig. 1). Values are averages $\pm$ 1 standard deviation from 200 bootstrapping runs. The bold values are the indices with the strongest correlation. EVI is the enhanced vegetation index, NDVI is the normalized difference vegetation index, RDVI is the renormalized difference vegetation index, SIWSI is the shortwave infrared water stress index. SIWSI<sub>12</sub> is based on the MODIS Bidirectional Reflectance Distribution Functions (NBAR) band 2 and band 5, whereas SIWSI<sub>16</sub> is based on MODIS NBAR band 2 and band 6.

Measurement site	$F_{opt}$					$\alpha$				
	EVI	NDVI	RDVI	SIWSI <sub>12</sub>	SIWSI <sub>16</sub>	EVI	NDVI	RDVI	SIWSI <sub>12</sub>	SIWSI <sub>16</sub>
ML-AgG	0.89 $\pm$ 0.02	0.87 $\pm$ 0.02	0.95 $\pm$ 0.01	<b>-0.95<math>\pm</math>0.01</b>	-0.93 $\pm$ 0.02	0.92 $\pm$ 0.02	0.91 $\pm$ 0.01	<b>0.96<math>\pm</math>0.01</b>	-0.94 $\pm$ 0.01	-0.88 $\pm$ 0.02
SN-Dah	0.92 $\pm$ 0.005	0.91 $\pm$ 0.01	0.96 $\pm$ 0.003	<b>-0.96<math>\pm</math>0.004</b>	-0.93 $\pm$ 0.01	0.89 $\pm$ 0.01	0.90 $\pm$ 0.01	<b>0.93<math>\pm</math>0.01</b>	-0.92 $\pm$ 0.01	-0.87 $\pm$ 0.01
SD-Dem	0.81 $\pm$ 0.01	0.78 $\pm$ 0.01	0.91 $\pm$ 0.01	<b>-0.93<math>\pm</math>0.01</b>	-0.90 $\pm$ 0.01	0.76 $\pm$ 0.02	0.73 $\pm$ 0.02	<b>0.86<math>\pm</math>0.01</b>	-0.82 $\pm$ 0.02	-0.79 $\pm$ 0.02
MA-Kem	0.77 $\pm$ 0.02	0.83 $\pm$ 0.02	0.95 $\pm$ 0.01	<b>-0.95<math>\pm</math>0.01</b>	-0.90 $\pm$ 0.02	0.69 $\pm$ 0.05	0.73 $\pm$ 0.04	<b>0.80<math>\pm</math>0.03</b>	-0.77 $\pm$ 0.03	-0.76 $\pm$ 0.03
NE-WaF	0.87 $\pm$ 0.02	0.81 $\pm$ 0.02	0.78 $\pm$ 0.02	<b>-0.90<math>\pm</math>0.01</b>	-0.80 $\pm$ 0.02	<b>0.89<math>\pm</math>0.01</b>	0.84 $\pm$ 0.01	0.85 $\pm$ 0.01	-0.88 $\pm$ 0.01	-0.79 $\pm$ 0.01
NE-WaM	0.41 $\pm$ 0.05	0.50 $\pm$ 0.04	<b>0.72<math>\pm</math>0.03</b>	-0.55 $\pm$ 0.04	-0.43 $\pm$ 0.05	0.72 $\pm$ 0.02	0.76 $\pm$ 0.02	<b>0.81<math>\pm</math>0.01</b>	-0.75 $\pm$ 0.01	-0.72 $\pm$ 0.01
All sites	0.86 $\pm$ 0.0	0.79 $\pm$ 0.0	<b>0.90<math>\pm</math>0.0</b>	0.75 $\pm$ 0.0	0.70 $\pm$ 0.0	0.83 $\pm$ 0.01	0.80 $\pm$ 0.01	<b>0.86<math>\pm</math>0.01</b>	0.62 $\pm$ 0.01	0.54 $\pm$ 0.01

**Table 3.** Statistics for the regression tree analysis. The regression tree analysis was used ~~for~~ ~~to~~ ~~study~~ ~~ing~~ relationships between intra-annual dynamics in the ~~the~~ photosynthetic capacity ( $F_{opt}$ ;  $F_{opt\_frac}$  for all sites) and quantum efficiency ( $\alpha$ ;  $\alpha_{frac}$  for all sites) and the explanatory variables for the six measurement sites (Fig. 1). The pruning level is the number of splits of the regression tree and an indication of complexity of the system.

Measurement site	Explanatory variables:					Pruning level	$R^2$
	1	2	3	4	5		
$F_{opt}$							
ML-AgG	SIWSI <sub>12</sub>	Tair	PAR	SWC		16	0.98
SN-Dah	SIWSI <sub>12</sub>	SWC	VPD	Tair	PAR	84	0.98
SD-Dem	SIWSI <sub>12</sub>	VPD	SWC	Tair	PAR	33	0.97
ML-Kem	SIWSI <sub>12</sub>	PAR	Tair	VPD		22	0.98
NE-WaF	SIWSI <sub>12</sub>	SWC	VPD	Tair		14	0.92
NE-WaM	RDVI	SWC	VPD	Tair		18	0.75
All sites	RDVI	SWC	Tair	VPD		16	0.87
$\alpha$							
ML-AgG	RDVI					3	0.95
SN-Dah	RDVI	VPD	SWC	Tair	PAR	21	0.93
SD-Dem	RDVI	SWC	PAR	Tair		16	0.93
ML-Kem	RDVI	Tair				4	0.75
NE-WaF	EVI	SWC	VPD			10	0.90
NE-WaM	RDVI	SWC	VPD	Tair		15	0.86
All sites	RDVI	SWC	VPD	Tair		16	0.84

**Table 4.** Annual peak values of quantum efficiency ( $\alpha_{\text{peak}}$ ;  $\mu\text{mol CO}_2 \mu\text{mol PAR}^{-1}$ ) and photosynthetic capacity ( $F_{\text{opt\_peak}}$ ;  $\mu\text{mol CO}_2 \text{m}^{-2} \text{s}^{-1}$ ) for the six measurement sites (Fig. 1). The peak values are the 2-week running mean with highest annual value.

Measurement site	Year	$\alpha_{\text{peak}}$	$F_{\text{opt\_peak}}$
ML-AgG	2007	0.0396	24.5
SN-Dah	2010	0.0638	50.0
	2011	0.0507	42.3
	2012	0.0480	39.2
	2013	0.0549	40.0
SD-Dem	2007	0.0257	16.5
	2008	0.0327	21.0
	2009	0.0368	16.5
ML-Kem	2007	0.0526	33.5
NE-WaF	2005	0.0273	18.2
	2006	0.0413	21.0
NE-WaM	2005	0.0252	10.6
	2006	0.0200	10.1
Average		0.0399	26.4

**Table 5.** Correlation matrix between annual peak values of photosynthetic capacity ( $F_{opt\_peak}$ ) and quantum efficiency ( $\alpha_{peak}$ ) and measured environmental variables. P is annual rainfall;  $T_{air}$  is yearly averaged air temperature at 2 m height; SWC is yearly averaged soil water content (% volumetric water content) measured at 0.1 m depth; Rh is yearly averaged relative humidity; VPD is yearly averaged vapour pressure deficit;  $R_g$  is yearly averaged incoming global radiation; N and C cont. are soil nitrogen and carbon contents;  $NDVI_{peak}$  is annual peak normalized difference vegetation index (NDVI);  $EVI_{peak}$  is annual peak enhanced vegetation index (EVI);  $RDVI_{peak}$  is annual peak renormalized difference vegetation index (RDVI);  $SIWSI_{12peak}$  is annual peak short-wave infrared water stress index based on MODIS NBAR band 2 and band 5; and  $SIWSI_{16peak}$  is annual peak short-wave infrared water stress index based on MODIS NBAR band 2 and band 6. Sample size was 13 for all except the marked explanatory variables.

Explanatory variable	$F_{opt\_peak}$	$\alpha_{peak}$
<b>Meteorological data</b>		
P (mm)	0.24±0.26	0.13±0.27
$T_{air}$ (°C)	-0.07±0.25	-0.01±0.25
SWC (%) <sup>a</sup>	0.33±0.25	0.16±0.27
Rh (%)	0.73±0.16*	0.60±0.19
VPD (hPa)	0.20±0.26	0.15±0.30
$R_g$ (W m <sup>-2</sup> )	-0.48±0.21	-0.41±0.24
<b>Biomass and edaphic data</b>		
Biomass (g DW m <sup>-2</sup> ) <sup>a</sup>	0.77±0.15*	0.74±0.14*
C3/C4 ratio	-0.05±0.26	0.06±0.30
N cont. (%) <sup>b</sup>	0.22±0.11	0.35±0.14
C cont. (%) <sup>b</sup>	0.89±0.06**	0.87±0.07**
<b>Earth observation data</b>		
$NDVI_{peak}$	0.94±0.05**	0.87±0.07**
$EVI_{peak}$	0.93±0.04**	0.87±0.07**
$RDVI_{peak}$	0.93±0.04**	0.89±0.07**
$SIWSI_{12peak}$	0.85±0.08**	0.84±0.08**
$SIWSI_{16peak}$	0.67±0.12*	0.65±0.15*
<b>Photosynthetic variables</b>		
$F_{opt}$	-	0.94±0.03**

<sup>a</sup>sample size equals 11.

<sup>b</sup>sample size equals 9.

\* significant at 0.05 level.

\*\* significant at 0.01 level



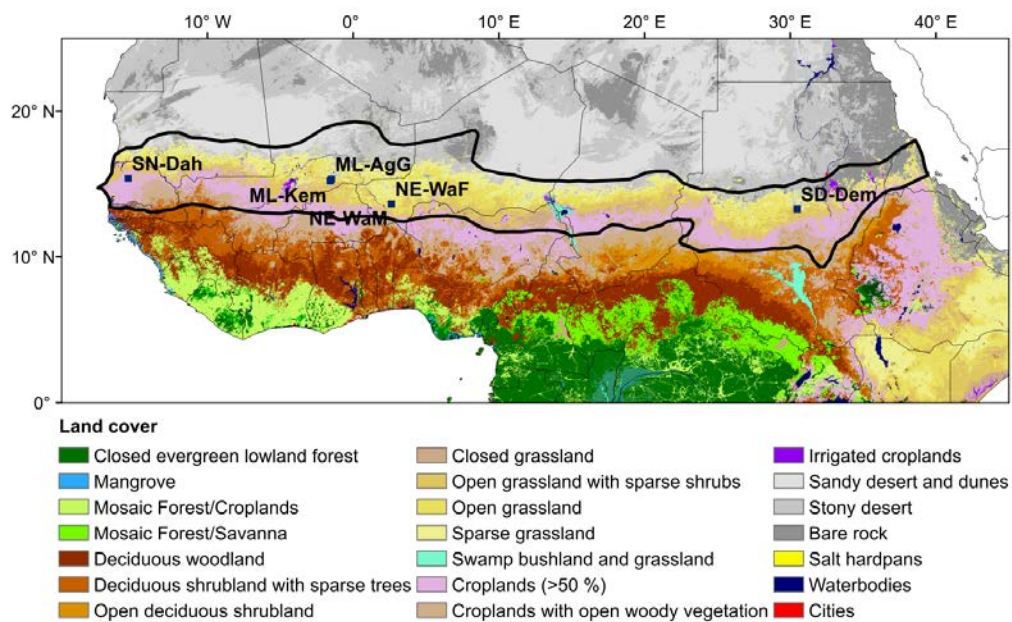
**Table 6.** Statistics regarding the evaluation of the gross primary production (GPP) model for the six measurement sites (Fig. 1). In situ and modelled GPP are averages  $\pm 1$  standard deviation. RMSE is the root-mean-squares-error, and slope, intercept and  $R^2$  are from the fitted ordinary least squares linear regression.

Measurement site	In situ GPP ( $\mu\text{mol CO}_2 \text{ m}^{-2} \text{ s}^{-1}$ )	Modelled GPP ( $\mu\text{mol CO}_2 \text{ m}^{-2} \text{ s}^{-1}$ )	RMSE ( $\mu\text{mol CO}_2 \text{ m}^{-2} \text{ s}^{-1}$ )	slope	Intercept ( $\mu\text{mol CO}_2 \text{ m}^{-2} \text{ s}^{-1}$ )	$R^2$
ML-AgG	5.35 $\pm$ 6.38	5.97 $\pm$ 5.80	2.48 $\pm$ 0.10	0.84 $\pm$ 0.003	1.46 $\pm$ 0.01	0.86 $\pm$ 0.002
SN-Dah	9.39 $\pm$ 10.17	8.87 $\pm$ 9.67	3.99 $\pm$ 1.34	0.88 $\pm$ 0.002	0.62 $\pm$ 0.01	0.85 $\pm$ 0.001
SD-Dem	4.26 $\pm$ 4.55	3.98 $\pm$ 3.90	3.15 $\pm$ 1.06	0.63 $\pm$ 0.003	1.31 $\pm$ 0.007	0.54 $\pm$ 0.02
ML-Kem	11.16 $\pm$ 8.02	10.52 $\pm$ 9.22	4.35 $\pm$ 1.23	1.02 $\pm$ 0.003	-0.82 $\pm$ 0.03	0.78 $\pm$ 0.002
NE-WaF	5.77 $\pm$ 4.17	6.63 $\pm$ 3.53	2.47 $\pm$ 1.05	0.70 $\pm$ 0.005	2.58 $\pm$ 0.02	0.69 $\pm$ 0.003
NE-WaM	3.04 $\pm$ 1.93	6.35 $\pm$ 3.47	4.12 $\pm$ 0.99	1.31 $\pm$ 0.004	2.37 $\pm$ 0.02	0.53 $\pm$ 0.003
Average	6.73 $\pm$ 7.72	7.02 $\pm$ 7.39	3.68 $\pm$ 0.55	0.83 $\pm$ 0.07	1.34 $\pm$ 0.82	0.84 $\pm$ 0.07

**Table 7.** The parameters for Eq. 13 that ~~was~~were used in the final gross primary production (GPP) model. RMSE is the root mean square error, and  $R^2$  is the coefficient of determination for the regression models predicting the different variables.

Parameter	Value	RMSE	$R^2$
$k_{Fopt}$	$79.6 \pm 6.3$	$5.1 \pm 1.3$	$0.89 \pm 0.05$
$m_{Fopt}$	$-7.3 \pm 3.2$		
$l_{Fopt}$	$3.51 \pm 0.19$	$0.15 \pm 0.02$	$0.88 \pm 0.06$
$n_{Fopt}$	$0.03 \pm 0.006$		
$\alpha$	$0.16 \pm 0.02$	$0.0069 \pm 0.0021$	$0.81 \pm 0.10$
$m_\alpha$	$-0.014 \pm 0.007$		
$l_\alpha$	$3.75 \pm 0.27$	$0.20 \pm 0.02$	$0.80 \pm 0.10$
$n_\alpha$	$0.02 \pm 0.007$		

## Figures



- 5 **Figure 1.** Land cover classes for the Sahel and the location of the six measurement sites included in the study. The land cover classes are based on multi-sensor satellite observations (Mayaux et al., 2003). The sites are Agoufou (ML-AgG), Dahra (SN-Dah), Demokeya (SD-Dem), Kelma (ML-Kem), Wankama Fallow (NE-WaF), and Wankama Millet (NE-WaM). The thick black line [isare](#) the borders of the Sahel based on the isohyets 150 and 700 mm of annual precipitation (Prince et al., 1995).

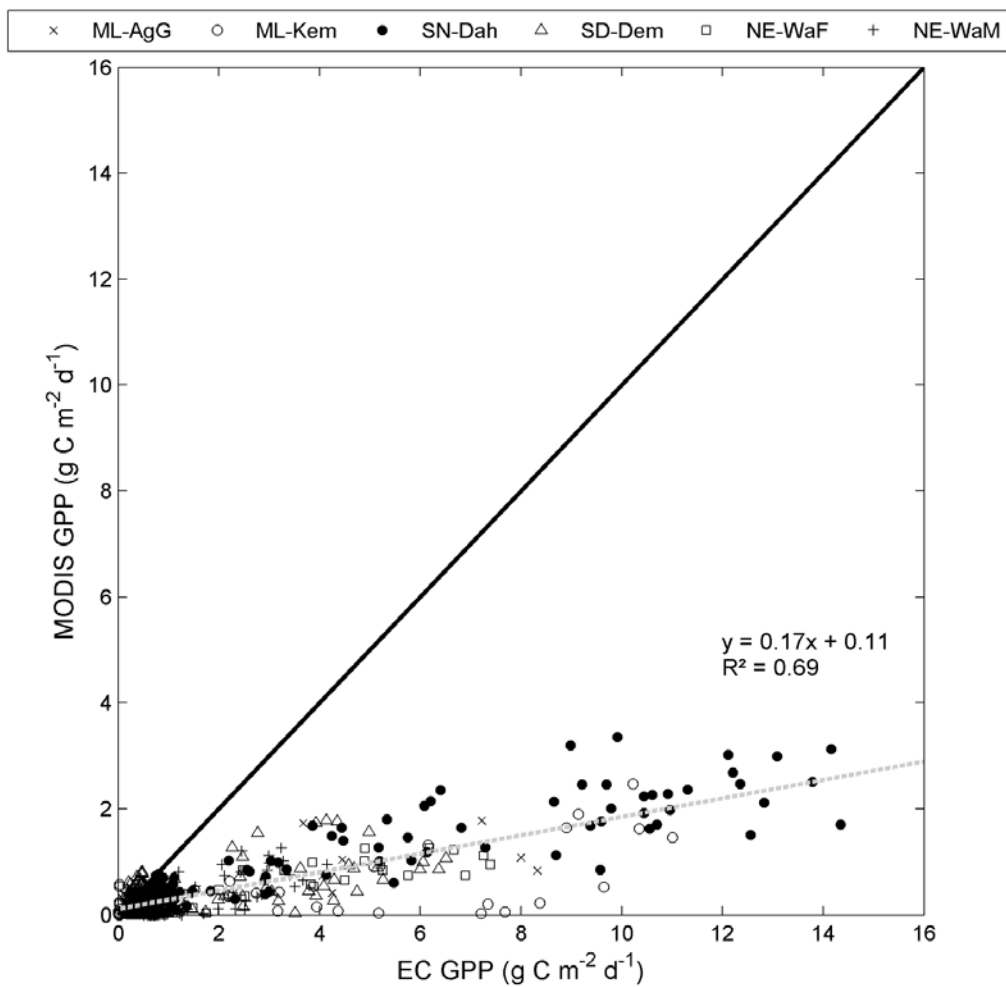


**Figure 2.** Evaluation of the MODIS based GPP product MOD17A2H (collection 6) against eddy covariance based GPP from the six measurement sites (Fig. 1) across the Sahel. The thick black line shows the one-to-one ratio, and the grey dotted line is the fitted ordinary least squares linear regression.

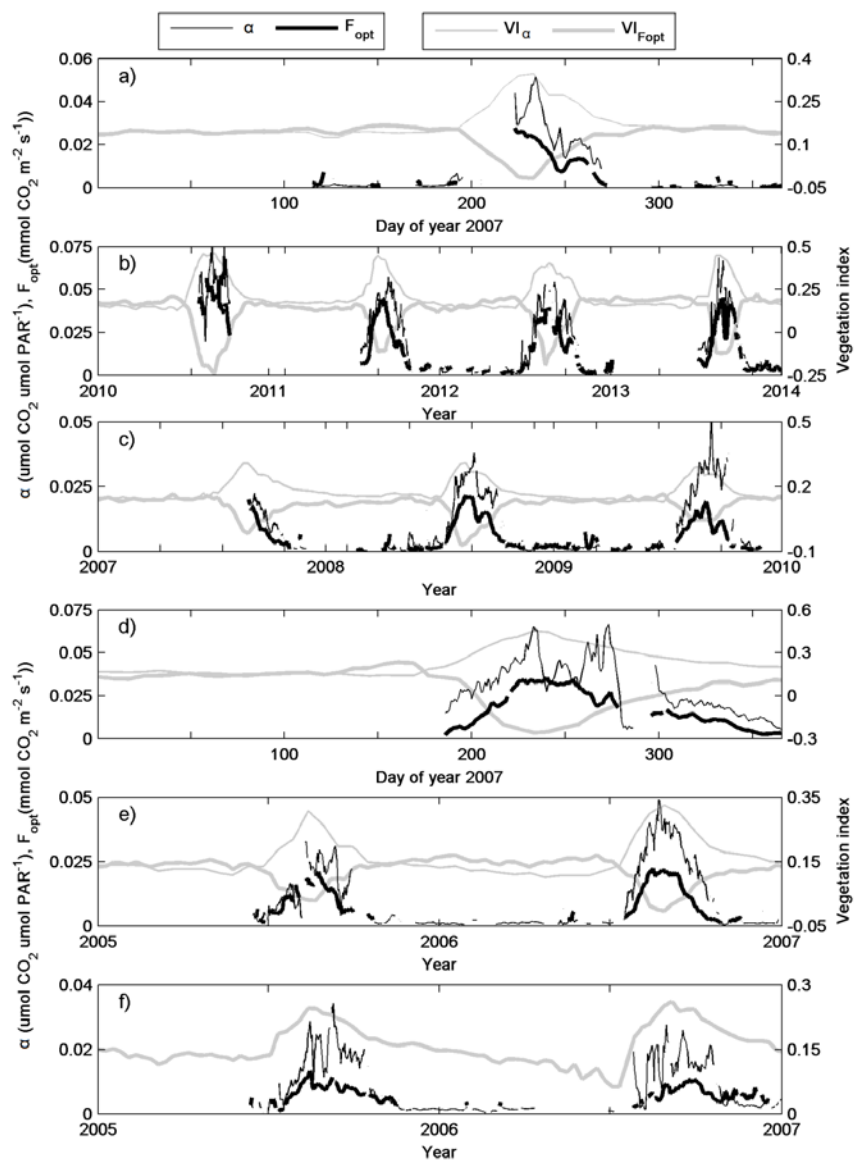


**Figure 3.** Dynamics in photosynthetic capacity ( $F_{opt}$ ) and quantum efficiency ( $\alpha$ ) for the six measurement sites. [Also included is also](#) dynamics in the vegetation indices with highest correlation to the intra-annual dynamics in  $F_{opt}$  ( $VI_{Fopt}$ ) and to quantum efficiency ( $VI_{\alpha}$ ) (Table 2). The sites are a) Agoufou (ML-AgG), b) Dahra (SN-Dah), c) Demokeya (SD-Dem), d) Kelma (ML-Kem), e) Wankama Fallow (NE-WaF) and f) Wankama Millet (NE-WaM).

5

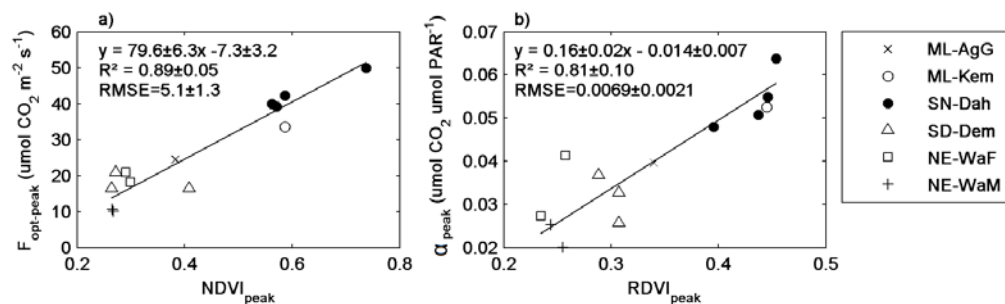


**Figure 4.** Scatter plots of annual peak values for the six measurement sites (Fig. 1) of a) photosynthetic capacity ( $F_{opt-peak}$ ) and b) quantum efficiency ( $\alpha_{peak}$ ) against peak values of normalized difference vegetation index ( $NDVI_{peak}$ ) and renormalized difference vegetation index ( $RDVI_{peak}$ ), respectively. The annual peak values were estimated by taking the annual maximum of a two-week running mean.

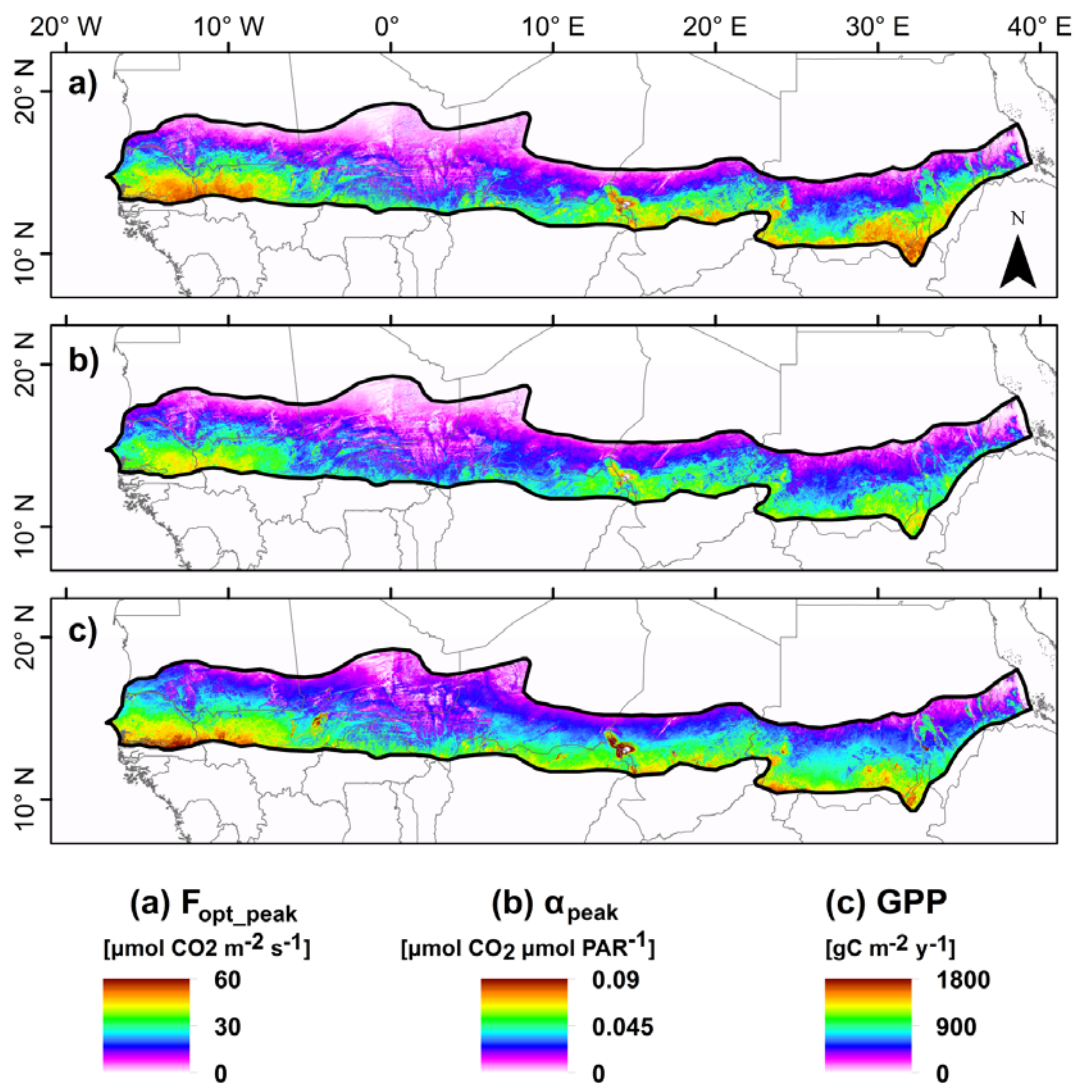


**Figure 5.** Maps of a) peak values of photosynthetic capacity ( $F_{opt\_peak}$ ) averaged for 2001-2014, b) peak values of quantum efficiency ( $\alpha_{peak}$ ) averaged for 2001-2014, and c) annual budgets of GPP averaged for 2001-2014.



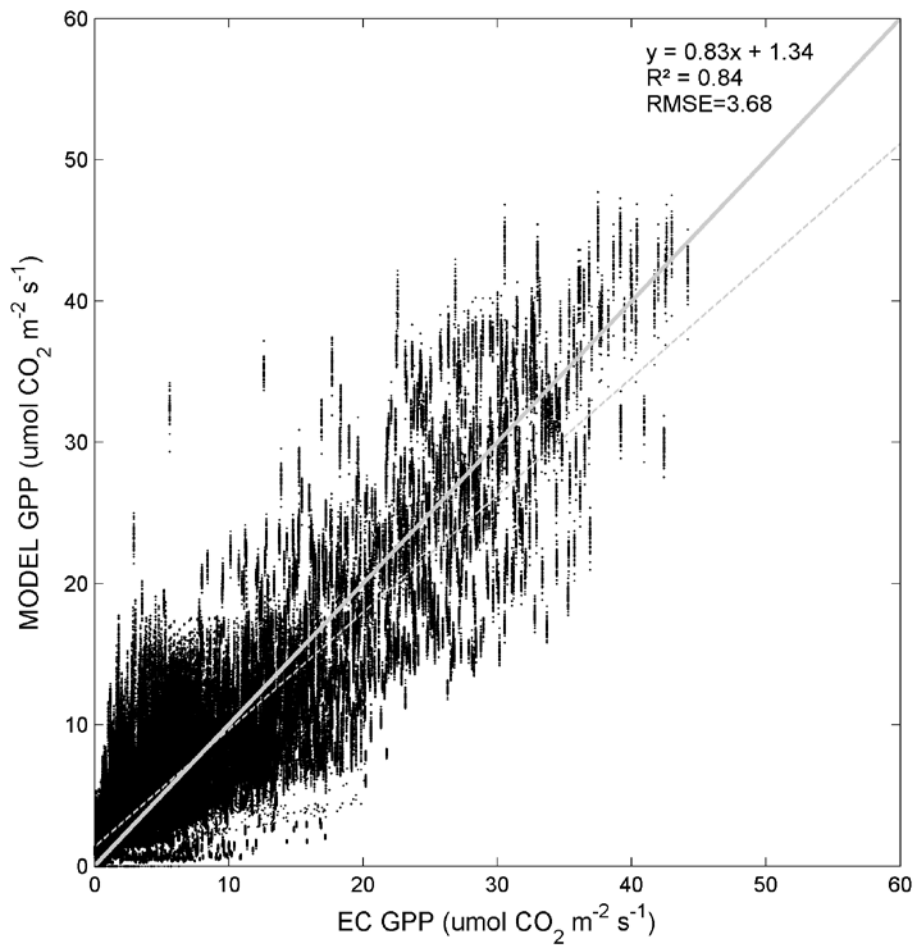


**Figure 6.** Evaluation of the modelled gross primary production (GPP) (Eq. 13) against in situ GPP from all six measurement sites across the Sahel. The thick grey line shows the one-to-one ratio, whereas the ~~dotted~~-thin dotted grey line is the fitted ordinary least squares linear regression.

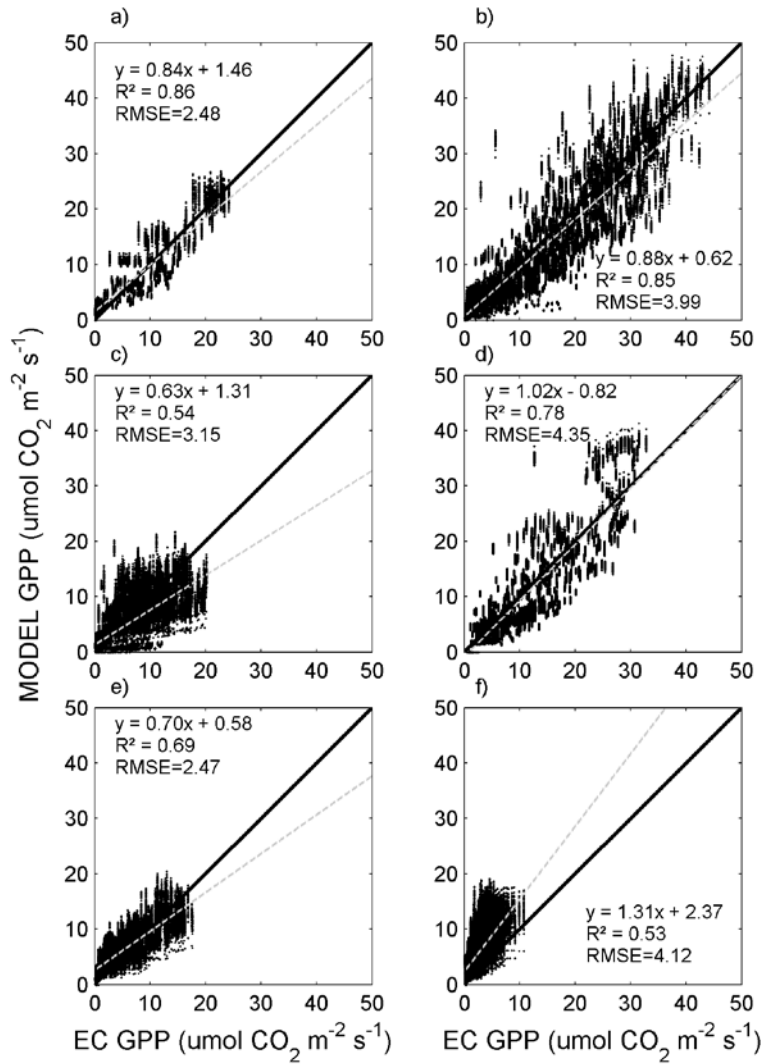


**Figure 7.** Evaluation of the modelled gross primary production (GPP) (Eq. 13) against in situ GPP for the six sites across Sahel (Fig. 1). The thick black line shows the one-to-one ratio, whereas the dotted thin grey line is the fitted ordinary least

square linear regression. The sites are a) Agoufou (ML-AgG), b) Dahra (SN-Dah), c) Demokeya (SD-Dem), d) Kelma (ML-Kem), e) Wankama Fallow (NE-WaF) and f) Wankama Millet (NE-WaM).